Biochemistry and Biophysics Reports 5 (2016) 453–467

Contents lists available at ScienceDirect

Biochemistry and Biophysics Reports

journal homepage: www.elsevier.com/locate/bbrep

Model of the pathway of –1 frameshifting: Kinetics

Ping Xie

Key Laboratory of Soft Matter Physics and Beijing National Laboratory for Condensed Matter Physics, Institute of Physics, Chinese Academy of Sciences, Beijing 100190, China

ARTICLE INFO

Article history:
Received 20 November 2015
Received in revised form
4 February 2016
Accepted 9 February 2016
Available online 10 February 2016

Keywords:
Ribosome
Translational regulation
Translation elongation
Protein synthesis
Virus

ABSTRACT

Programmed –1 translational frameshifting is a process where the translating ribosome shifts the reading frame, which is directed by at least two stimulatory elements in the mRNA—a slippery sequence and a downstream secondary structure. Despite a lot of theoretical and experimental studies, the detailed pathway and mechanism of the –1 frameshifting remain unclear. Here, in order to understand the pathway and mechanism we consider two models to study the kinetics of the –1 frameshifting, providing quantitative explanations of the recent biochemical data of Caliskan et al. (Cell 2014, 157, 1619–1631). One model is modified from that proposed by Caliskan et al. and the other is modified from that proposed in the previous work to explain the single-molecule experimental data. It is shown that by adjusting values of some fundamental parameters both models can give quantitative explanations of the biochemical data of Caliskan et al. on the kinetics of EF-G binding and dissociation and on the kinetics of movement of tRNAs inside the ribosome. However, for the former model some adjusted parameter values deviate significantly from those determined from the available single-molecule experiments, while for the latter model all parameter values are consistent with the available biochemical and single-molecule experimental data. Thus, the latter model most likely reflects the pathway and mechanism of the –1 frameshifting.

1. Introduction

Programmed ribosomal frameshifting is a process where specific signals in the messenger RNA (mRNA) direct the translating ribosome to shift the reading frame. When the reading frame is shifted in the 3′ direction or the 5′ direction by one nucleotide, it is called +1 or −1 frameshifting, respectively. The classic example of the −1 frameshifting contains two stimulatory signals in the mRNA—a slippery sequence and a downstream secondary structure [1–3]. In some prokaryotic cases such as the *dnaX* –1 frameshifting mRNA, three stimulatory signals—an upstream, internal Shine-Dalgarno (SD) sequence, the slippery sequence and the downstream mRNA duplex —are necessary to stimulate the efficient −1 frameshifting [3].

Recently, using single-molecule fluorescence to track directly the compositional and conformational dynamics of individual ribosomes at each codon, Chen et al. [4] studied the −1 frameshifting during translation of the *dnaX* –1 frameshift mRNA. The dynamics of long pausing associated with the −1 frameshifting and the dynamics of EF-G and tRNA samplings in the long-paused state were studied in detail [4]. Using single-molecule fluorescence resonance energy transfer (FRET), Kim et al. [5] found that the pretranslocation ribosomal complexes exhibit multiple fluctuations between the non-rotated and rotated states before undergoing mRNA translocation during translation of the *dnaX* –1 frameshift mRNA even at saturating EF-G. With the PURExpress in vitro translation system, Yan et al. [6] found that the ribosomes can undergo several translocation excursions to shift reading frame and access a range of codon positions. Caliskan et al. [7] made detailed biochemical studies on the kinetics of the translocation reactions that govern the –1 frameshifting in the system with a modified IBV 1a/1b gene fragment (see Fig. S1a). They studied the kinetics of EF-G binding and dissociation by monitoring the change in the fluorescence resonance energy transfer (FRET) between a FRET donor (Alexa 488, Alx) placed on ribosomal protein L12 that is known to recruit translation factors to the ribosome and a non-fluorescent FRET acceptor (QSY9) in the G domain of EF-G, and studied the kinetics of movement of tRNAs inside the ribosome by monitoring the change in the fluorescence of fluorescein (Flu) labeled at $tRNA^{Leu}$ and the change in FRET between S13(AttoQ) of the 30S subunit and the $tRNA^{Leu}$(Flu). Based on their biochemical data, they proposed a model for the pathway of the –1 frameshifting (see Fig. S1). However, a quantitative study based on the model indicates that the calculated results are not consistent with the biochemical data (see Section S1). Thus, to understand the pathway and mechanism of the –1 frameshifting, a modified model or a new model that can provide quantitative explanations of the biochemical data [7] is necessary.

E-mail address: pxie@aphy.iphy.ac.cn

http://dx.doi.org/10.1016/j.bbrep.2016.02.008

Several models have been proposed to address the −1 frameshifting pathway and mechanism. It was proposed that the −1 frameshifting can occur at the aminoacyl-tRNA accommodation step [8,9], at the translocation step [10,11], or at both of the two steps [12]. A systematical analysis proposed that while the −1 frameshifting can occur during the translocation step, during the period after the posttranslocation and before the binding of the aminoacyl-tRNA and during the period after the codon recognition and before the peptidyl transfer, the frameshifting takes place mainly during the translocation over the slippery sequence [13]. In the previous work [14], a new model of the −1 frameshifting was proposed to quantitatively explain the recent single-molecule experimental data of Chen et al. [4] on the dynamics of long pausing that is associated with the −1 frameshifting. The single-molecule FRET data of Kim et al. [5] and the experimental data of Yan et al. [6] were also explained [14,15]. In the models [8–14] only the intersubunit rotations between the 50S and 30S subunits are considered. However, structural and biochemical studies showed that besides the intersubunit rotations, the intrasubunit rotations of the 30S head relative to the 30S body are also involved in the translocation of the tRNA-mRNA complex in the 30S subunit [16–20]. As the −1 frameshifting occurs mainly during the translocation step, it is necessary to incorporate the intrasubunit 30S head rotations in the model of the −1 frameshifting. Moreover, with the previous model by considering only the intersubunit rotations, although the experimental data of Chen et al. [4], Kim et al. [5] and Yan et al. [6] can be explained well [14], the biochemical data of Caliskan et al. [7] on the kinetics of the −1 frameshifting, which are monitored by labeling the ribosomal protein of the 30S head, cannot be explained.

In this work, to understand the detailed molecular mechanism and pathway of the −1 frameshifting and to quantitatively explain the biochemical data of Caliskan et al. [7], we consider two models, with one being modified from the model proposed by Caliskan et al. [7] and another one being modified from the previous model [14] by also considering the intrasubunit 30S head rotations. It is shown that by adjusting values of some fundamental parameters both modified models can give quantitative explanations of the biochemical data of Caliskan et al. [7]. However, for the former model some adjusted parameter values deviate significantly from those determined from the single-molecule experiments of Chen et al. [4], while for the latter model all of the adjusted parameter values are consistent with the available biochemical and single-molecule experimental data. Thus, we believe that the latter model most likely reflects the pathway and mechanism of the −1 frameshifting.

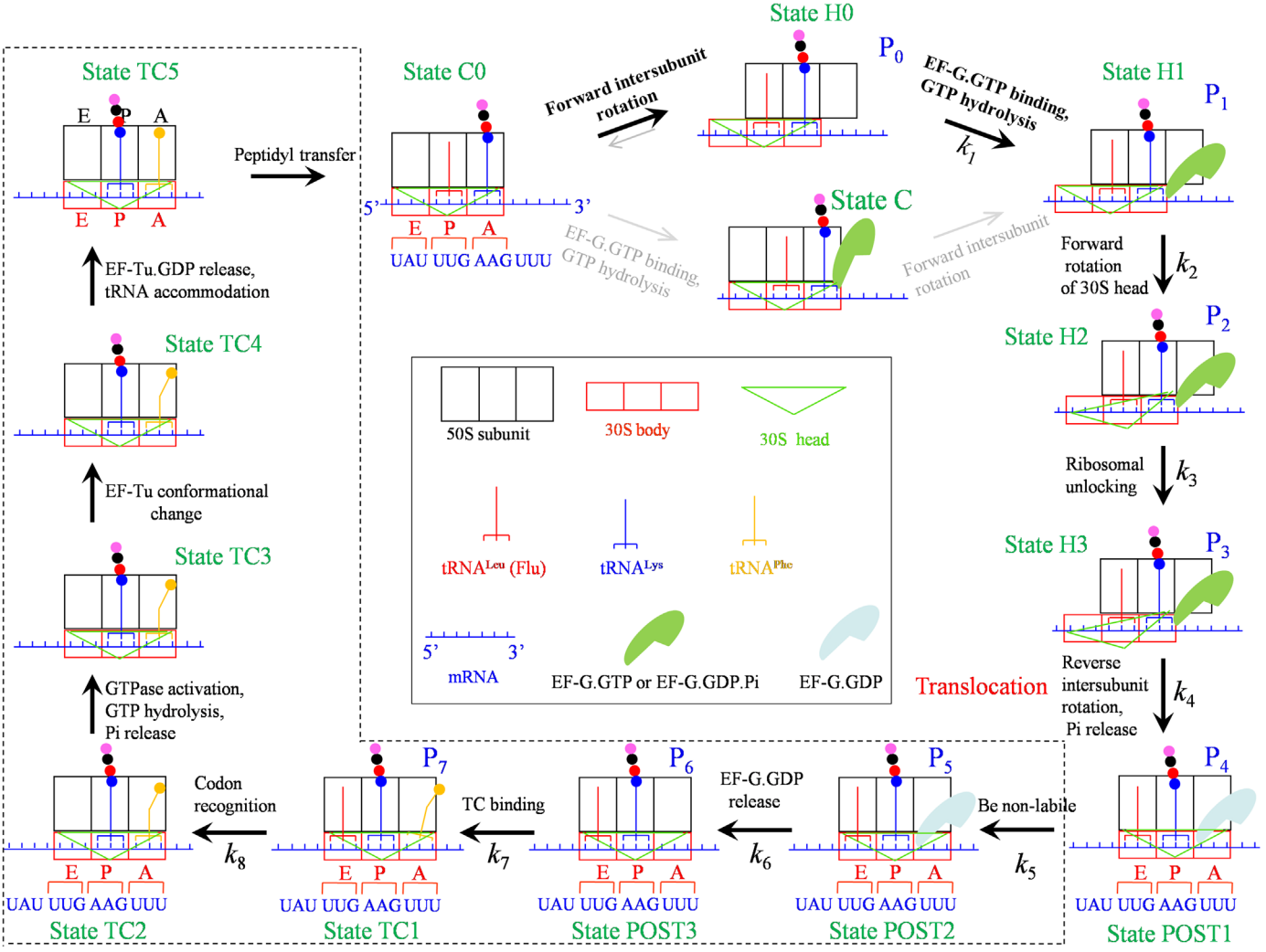

Fig. 1. Schematic representation of the elongation pathway for ribosome translation of mRNA lacking both the slippery sequence and downstream secondary structure (see text for detailed description). Note that EF-G bound to the non-rotated pretranslocation state (State C) is in the compact conformation while EF-G bound to the rotated pretranslocation state (State H1, State H2, State H3) and bound to the non-rotated posttranslocation state (State POST1, State POST2) is in the elongated conformation [28].

2. Models

To model the pathway and mechanism of the –1 translational frameshifting in the classic systems containing the two stimulatory elements in the mRNA—the slippery sequence and downstream secondary structure, we firstly present the model of the elongation pathway for the simple case of translation of the mRNA lacking both stimulatory elements. As done in Caliskan et al. [7], the mRNA construct that contains both slippery sequence and pseudoknot is designated as +/+ (see Fig. S1a), while the construct that lacks both stimulatory elements is designated as –/–.

2.1. Model of the elongation pathway for translation of the mRNA lacking both two stimulatory elements

Based on the models proposed in the previous work [14,21], the elongation pathway of the translation of –/– mRNA by incorporating 30S head rotation is schematically shown in Fig. 1, where the system is the same as that used in Caliskan et al. [7]. Just after the peptidyl transfer, the peptidyl-tRNA (fMetTyrLeuLys-tRNA^{Lys}) is in the A/A site and deacylated tRNA (tRNA^{Leu}) in the P/P site (State C0). Before EF-G.GTP binding, the ribosomal complex transits spontaneously between State C0 and hybrid State H0, with the majority being in State H0 [22–24]. EF-G.GTP can bind to both State C0 and State H0 [25–28]. (i) If EF-G.GTP binds to State H0 (becoming State H1), after rapid GTP hydrolysis to GDP.Pi form smaller conformational changes in EF-G cause the tip of domain IV to shift towards and interact with the decoding center in the 30S subunit, inducing the counterclockwise (forward) rotation of the 30S head relative to the 30S body (State H2) [16]. The forward 30S head rotation then induces the ribosomal unlocking (State H3), widening the mRNA channel and causing the 30S subunit to transit from closed to open conformation [14]. The subsequent reverse intersubunit rotation together with the reverse rotation of the 30S head[1], which are facilitated by the ribosomal unlocking, makes the 30S subunit move downstream relative to the mRNA that is coupled with the two tRNAs by one codon, while the high affinity of the 50S E and P sites for the two tRNAs [38,39] fixes the two tRNAs to the 50S subunit, with State H3 transiting to posttranslocation state (State POST1). Facilitated by the ribosomal unlocking, Pi is also released rapidly but independently of the reverse intersubunit rotation [40]. In State POST1 with the non-rotated 30S head, the mRNA channel in the 30S subunit becomes tight[2]. (ii) If EF-G.GTP binds to State C0, EF-G.GTP facilitates State C transiting to State H1 [24], where the forward 30S head rotation occurs (State H2), inducing the ribosomal unlocking (State H3). The subsequent reverse intersubunit rotation makes State H3 transit to State POST1.

In State POST1, the "canonical" P/P-site peptidyl-tRNA induces the labile ribosome to be non-labile (State POST2) [3], accelerating EF-G.GDP release (State POST3) and prohibiting EF-G.GTP binding. Thus, only the ternary complex (EF-Tu.GTP.Phe-tRNA^{Phe}) can bind efficiently to the ribosome with an open 30S subunit (State TC1) [14]. The subsequent codon recognition (State TC2) induces closing of the 30S subunit [14] and triggers GTP hydrolysis and Pi release (State TC3), resulting in conformational change of EF-Tu (State TC4). EF-Tu.GDP is then released and the aminoacyl-tRNA is accommodated into the full A/A state (State TC5). Then, the peptidyl transfer leads to State C0.

The available experimental data showed that before EF-G.GTP binding to State C0 or to State H0 the majority of the ribosomal complexes are in State H0 [22–24]. Thus, in this work we consider that in the elongation cycle the transitions occur mainly along State C0 to State H0 to State H1, as done in the previous work [14].

2.2. Models of the pathway of –1 frameshifting

Based on the model of the translation of –/– mRNA shown in Fig. 1 and the models of –1 frameshifting proposed before [7,14], we consider two models here to quantitatively explain the biochemical data of Caliskan et al. [7]. The two models are described as follows.

2.2.1. Model I

To explain their biochemical data, Caliskan et al. [7] proposed a model for the pathway of the –1 frameshifting (see Fig. S1). Based on the model of Fig. 1, we modify the model of Fig. S1, as shown in Fig. 2 which is called Model I. As the majority of the translating ribosomes frameshift (over 75%) [7], for simplicity, in Fig. 2 only the –1-frame pathway is shown.

After the binding of EF-G.GTP to State H0 and then GTP hydrolysis to GDP.Pi (State H1), the forward 30S head rotation occurs (State H2), inducing the ribosomal unlocking (State H3). Due to the resistance of the downstream pseudoknot, the subsequent reverse intersubunit rotation, which is accompanied by the reverse 30S head rotation, causes an incomplete translocation at the slippery sequence, with the two tRNAs (tRNA^{Leu} and fMetTyrLeuLys-tRNA^{Lys}) making a –1 shift of reading frames from UUA_AAG to UUU_AAA (State POST1). Then, the ribosome becomes non-labile (State POST2), accelerating EF-G.GDP release (State POST3). After the binding of the ternary complex EF-Tu.GTP.Val-tRNA^{Val} (State TC1), the codon recognition (State TC2) and the aminoacyl-tRNA accommodation (State TC5), the peptidyl transfer takes place (State C0). Then, the spontaneous forward intersubunit rotation induces the ribosomal complex returning to State H0.

The 0-frame pathway is similar to the –1-frame pathway and the branching occurs during the transition from State H3 to the posttranslocation state.

2.2.2. Model II

In the previous work [14], we proposed a model of –1 frameshifting, where the 30S head rotations were not included for simplicity. Here, based on the model of Fig. 1 we modify the previous model [14] by considering the 30S head rotations to quantitatively explain the in vitro biochemical data of Caliskan et al. [7]. The modified model is called Model II, which is schematically shown in Figs. 3 and 4.

In Fig. 3, the transitions from State C0 through State H3 are the same as those in Fig. 1 or Fig. 2. Due to the resistance of the downstream pseudoknot, the subsequent reverse intersubunit rotation can bring about the transition of State H3 to one of the following three states at the slippery sequence. One is the canonical posttranslocation state (State POST1), where the 30S subunit moves downstream by unwinding three mRNA base pairs while two tRNAs are fixed to the 50S subunit by the high affinity between them [38,39]. Another is the classical non-rotated pretranslocation state (State FC), where the 50S subunit moves relative to the two tRNAs by overcoming the high affinity between

[1] Note 1. As discussed in detail elsewhere [21], the available structural data showed that the ribosome complexed with tRNA with the non-rotated intersubunit conformation always has a non-rotated 30S head [29–37]. Thus, it was argued that the reverse intersubunit rotation is accompanied or immediately followed by the reverse 30S head rotation [21]

[2] Note 2. As the forward rotated 30S head causes the ribosomal unlocking, opening the mRNA channel [21], and the non-rotated intersubunit conformation always has a non-rotated 30S head [29–37], it is thus noted that the ribosomal complex with the non-rotated intersubunit conformation and non-rotated 30S head has a tight mRNA channel [21].

[3] Note 3. In the literature, the ribosome in the "non-labile" state is usually called in the "locking" state. Here, for distinguishing from the "unlocking" state mentioned above, we use the "non-labile" instead of "locking".

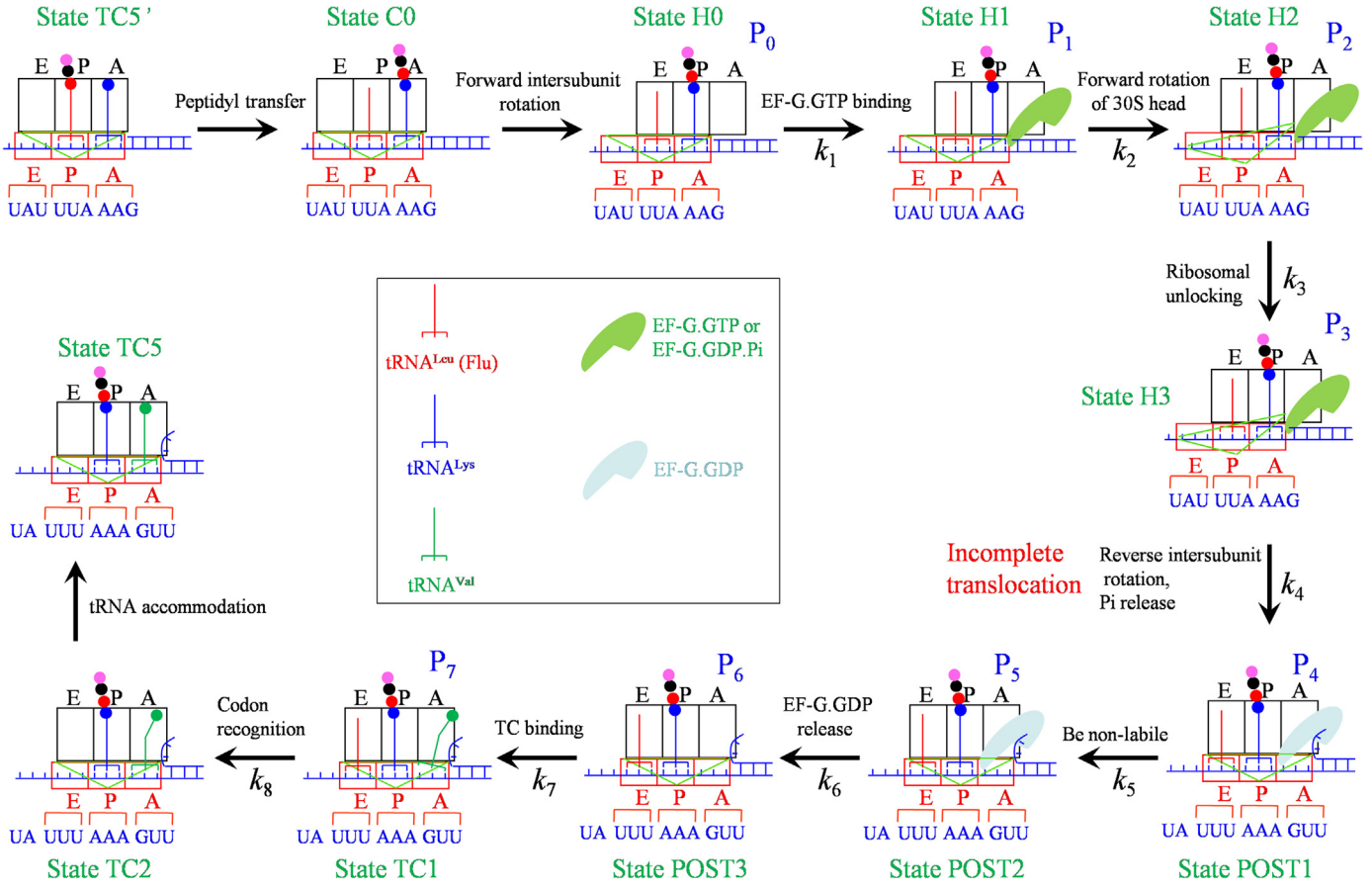

Fig. 2. Schematic representation of Model I for the pathway of –1 frameshifting, which is modified from the model proposed by Caliskan et al. [7] (see text for detailed description). Here, only the –1 frameshifting pathway is shown. Note that EF-G in State H1, State H2, State H3, State POST1 and State POST2 is in the elongated conformation.

them while the mRNA duplex prevents the 30S subunit from moving downstream [41,42]. The third is the non-canonical posttranslocation state (State LP), where both the 30S subunit moves downstream by unwinding two mRNA base pairs and shifting reading frames of the two tRNAs from UUA_AAG to UUU_AAA and the 50S subunit moves relative to the mRNA by bending the two tRNAs due to their high affinity for the 50S subunit [38,39] and the codon-anticodon interaction with codons UUU_AAA[4]. From State POST1 the transitions to State C0 are similar to those shown in Fig. 1 (inside the region bounded by broken lines). However, it is noted that the pulling on the mRNA that arises from the annealing tendency of the unwound mRNA base pairs of strong interactions would cause the codon in the 30S A to bias towards the 3′ direction; and this may reduce the rates of codon recognition and tRNA accommodation compared to those of translation of –/– mRNA, prolonging Phe incorporation [7]. In State FC with the non-rotated 30S head, the mRNA channel becomes tight and EF-G.GDP facilitates the labile State FC transiting to rotated State FH. After EF-G.GDP release, EF-G.GTP binding, GTP hydrolysis and then 30S head rotation, State FH becomes State H2. In State LP with the non-rotated 30S head, the mRNA channel becomes tight. The bent P/P-site peptidyl-tRNA cannot induce efficiently the ribosome to be non-labile and EF-G.GDP facilitates the labile ribosome transiting to the non-canonical rotated state (State FS).

From State FS the transition pathway to State C0 is schematically shown in Fig. 4 [14]. After EF-G.GDP release, either EF-G.GTP or the ternary complex can bind to State FS1. If EF-G.GTP binds, in the open conformation of the 30S subunit GTP hydrolysis has a low efficiency to induce the forward 30S head rotation. Without the ribosomal unlocking, the ribosome is kept rotated during the cycle of EF-G.GTP binding through EF-G.GDP release. Then, consider the binding of the ternary complex EF-Tu.GTP.Val-tRNA^{Val} (State FS2)[5]. The codon recognition induces the 30S subunit to transit to closed conformation, triggering GTP hydrolysis and Pi release (State FS3), followed by aminoacyl-tRNA accommodation and EF-Tu.GDP release (State FS4). During the slow codon recognition in the non-canonical rotated state, the aminoacyl-tRNA can be dissociated with a large probability, returning to State FS1. Thus, multiple bindings of the ternary complex can occur in the non-canonical rotated state [4].

In State FS3 if the aminoacyl-tRNA is dissociated without completion of the accommodation (State FS8), since the 30S subunit is in the closed conformation, the ternary complex cannot bind efficiently to State FS8 whereas EF-G.GTP can bind efficiently. GTP hydrolysis induces efficiently the forward 30S head rotation and in turn induces the ribosomal unlocking (State FS9), facilitating the reverse intersubunit rotation. Due to the specific affinity of

[4] Note 4. Since in State LP the deacylated tRNA^{Leu} forms codon-anticodon interaction with codon UUU, the deacylated tRNALeu has a low probability to dissociate from the E/E site. By contrast, in the previous work [14], in State LP the deacylated tRNA d oes not form codon-anticodon interaction with codon XXX, the deacylated tRNA has a large probability to dissociate from the E/E site.

[5] Note 5. Consider that the ternary complex EF-Tu.GTP.Phe-tRNA^{Phe} binds, with tRNA^{Phe} cognate to codon UUU. Because two tRNAs form codon-anticodon interaction with codons UUU_AAA, the codon recognition of tRNA^{Phe} to codon UUU would have a low probability to drive the two tRNAs to shift the frames from codons UUU_AAA to codons UUA_AAG, and thus the ternary complex would dissociate with a high probability. This is different from that studied in the previous work [14].

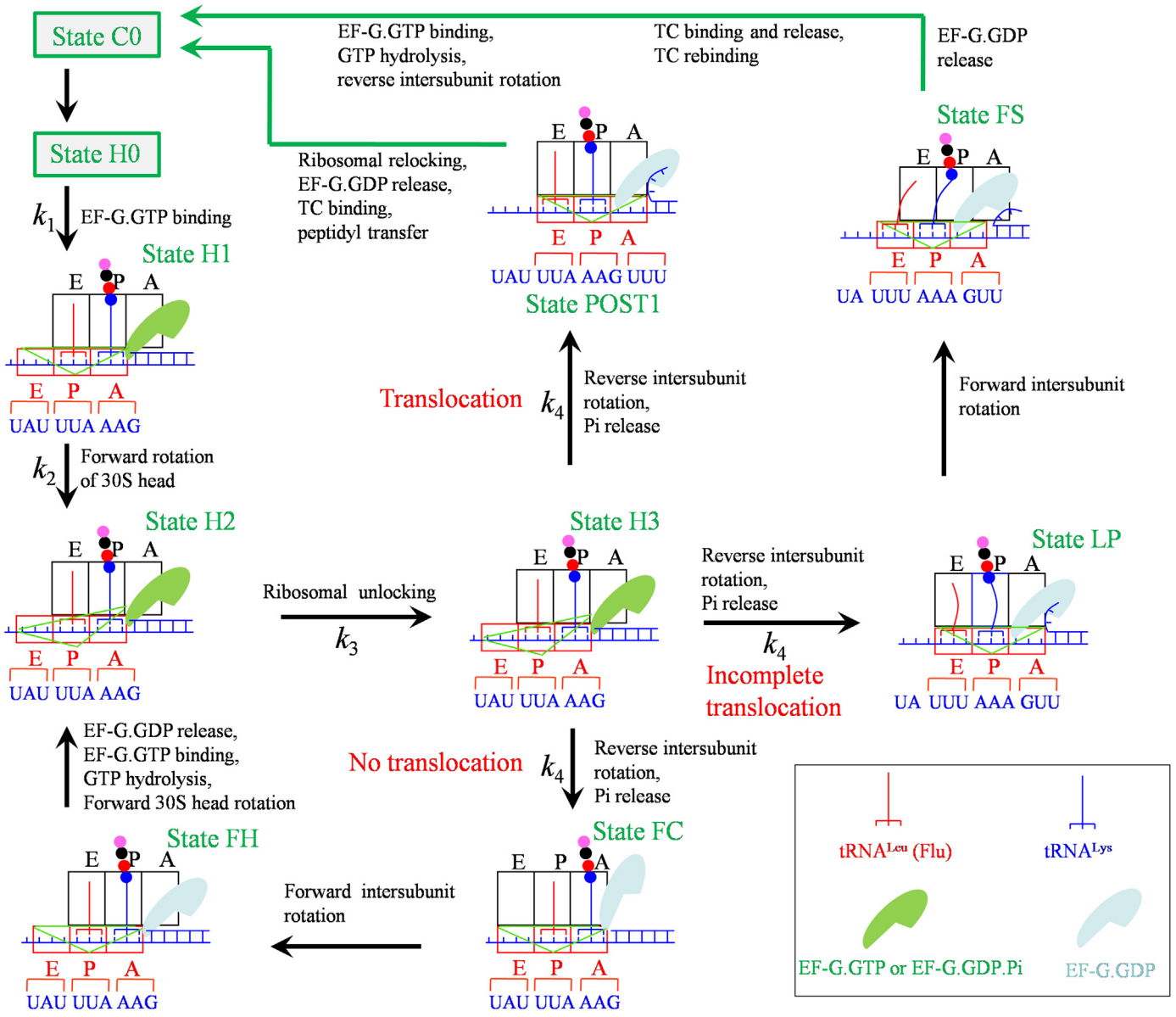

Fig. 3. Schematic representation of Model II for the pathway of −1 frameshifting, which is modified from the model proposed in the previous work (see text for detailed description) [14]. The transitions from State POST1 to State C0 are similar to those (the transitions inside the region bounded by broken lines) shown in Fig. 1. The transitions from State FS to State C0 are shown in Fig. 4. Note that EF-G in State FC is in the compact conformation while in State H1, State H2, State H3, State POST1, State FH, State LP and State FS is in the elongated conformation.

the 50S P site for the peptidyl-tRNA and the resistance of the mRNA duplex to the downstream movement of the 30S subunit, the reverse intersubunit rotation causes State FS9 transiting to State FS10. The transitions from State FS10 through State C0 are similar to those (inside the region bounded by broken lines) in Fig. 1. In State FS3 if the accommodation is completed without aminoacyl-tRNA dissociation (State FS4), EF-G.GTP binding and then GTP hydrolysis (State FS5) induces efficiently the forward 30S head rotation and in turn induces the ribosomal unlocking (State FS6), facilitating the reverse intersubunit rotation, with State FS6 transiting to State FS7, where the canonical P/P-site peptidyl-tRNA induces the ribosome to be non-labile. After EF-G.GDP release and the peptidyl transfer, the ribosomal complex returns to Sate C0.

3. Equations

We study the change in FRET between L12 and EF-G, the change in the fluorescence of tRNA^{Leu}(Flu), and the change in FRET between S13(AttoQ) and tRNA^{Leu}(Flu) during translation of both −/− mRNA and +/+ mRNA, in order to explain quantitatively the in vitro biochemical data of Caliskan et al. [7]. As in the experiment [7], we take time $t=0$ corresponding to State H0 (Figs. 1 – 3) to study the change in FRET between L12 and EF-G, where tRNA^{Leu}(Flu) is located in the P/E sites and fMetTyrLeuLys-tRNA^{Lys} in the A/P sites, and the reaction is ended with the EF-G.GDP release from the ribosome. To study the changes of tRNA^{Leu}(Flu) fluorescence and FRET between S13(AttoQ) and tRNA^{Leu}(Flu), the time $t=0$ corresponds to the moment just after the binding of EF-G.GTP to State H0, i.e., State H1. For the case of one round of translocation, the reaction is ended with the Lys incorporation and the ribosomal complex is in the posttranslocation state with EF-G.GDP release. For the case of two rounds of translocation, the reaction is ended with the Phe incorporation for −/− mRNA and is ended with Val (−1 frame) or Phe (0 frame) incorporation for +/+ mRNA.

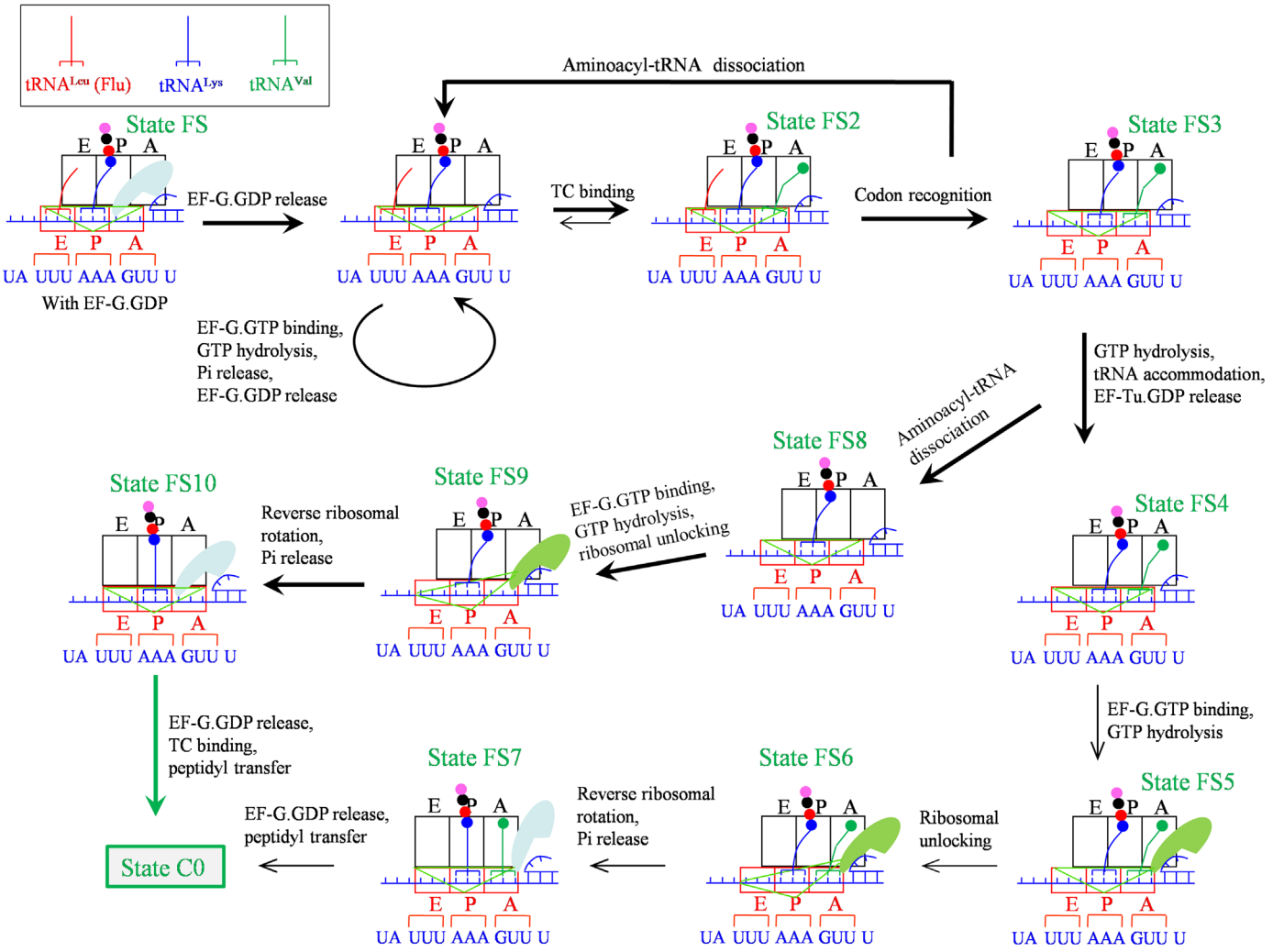

Fig. 4. Schematic representation of the pathway after entering into the non-canonical rotated state in Model II (see text for detailed description) [14]. State FS is the same as that shown in Fig. 3. Note that EF-G in State FS, State FS5, State FS6, State FS9 and State FS10 is in the elongated conformation while in State FS7 is in the compact conformation.

3.1. Equations for translation of –/– mRNA

In the pathway of Fig. 1, we denote by P_i ($i = 0, 1, \ldots, 7$) the probabilities of State H0, State H1, State H2, State H3, State POST1, State POST2, State POST3 and State TC1, respectively. For the case of two rounds of translocation, after the codon recognition (State TC2), due to the allosteric cooperation between the A and E sites $tRNA^{Leu}$(Flu) is considered to dissociate rapidly [43–45] if it has not been dissociated yet. Thus, for simplicity, we do not need to consider the transitions after the codon recognition in our studies of the changes of $tRNA^{Leu}$(Flu) fluorescence and FRET between S13 and $tRNA^{Leu}$(Flu).

Based on the pathway of Fig. 1, the change in FRET between L12 and EF-G can be characterized by

$$F_{EF-G} \propto P_0 + P_6, \tag{1}$$

where P_0 and P_6 are calculated from the following equations

$$\frac{dP_0(t)}{dt} = -k_1P_0(t), \tag{2}$$

$$\frac{dP_1(t)}{dt} = k_1P_0(t) - k_2P_1(t), \tag{3}$$

$$\frac{dP_2(t)}{dt} = k_2P_1(t) - k_3P_2(t), \tag{4}$$

$$\frac{dP_3(t)}{dt} = k_3P_2(t) - k_4P_3(t), \tag{5}$$

$$\frac{dP_4(t)}{dt} = k_4P_3(t) - k_5P_4(t), \tag{6}$$

$$\frac{dP_5(t)}{dt} = k_5P_4(t) - k_6P_5(t), \tag{7}$$

$$\frac{dP_6(t)}{dt} = k_6P_5(t) \tag{8}$$

The initial conditions (at $t = 0$) for Eqs. (2)–(8) are imposed as follows: $P_0(0) = 1$ and $P_i(0) = 0$ ($i = 1, 2, \ldots, 6$).

Based on the pathway of Fig. 1, the changes of $tRNA^{Leu}$(Flu) fluorescence and FRET between S13 and $tRNA^{Leu}$(Flu) for the case of one round of translocation can be resorted to the following equations

$$\frac{dP_1(t)}{dt} = -k_2P_1(t), \tag{9}$$

$$\frac{dP_2(t)}{dt} = k_2P_1(t) - k_3P_2(t), \tag{10}$$

$$\frac{dP_3(t)}{dt} = k_3P_2(t) - k_4P_3(t), \tag{11}$$

$$\frac{dP_4(t)}{dt} = k_4P_3(t) - k_5P_4(t) - k_dP_4(t), \tag{12}$$

$$\frac{dP_5(t)}{dt} = k_5P_4(t) - k_6P_5(t) - k_dP_5(t), \tag{13}$$

$$\frac{dP_6(t)}{dt} = k_6P_5(t) - k_dP_6(t), \tag{14}$$

where k_d is the rate of tRNA^{Leu}(Flu) dissociation after the post-translocation. The initial conditions (at $t=0$) are imposed as follows: $P_1(0)=1$ and $P_i(0)=0$ ($i=2, \ldots, 6$). Considering that different conformations of the ribosomal complex should give different fluorescence intensities of tRNA^{Leu}(Flu), as done before [46], the change in the fluorescence of tRNA^{Leu}(Flu) is calculated by

$$Flu_1(t) \propto \left[P_1(t) + P_2(t) + P_3(t)\right] + A_1P_4(t) + A_2P_5(t) + A_3P_6(t), \tag{15}$$

where A_1, A_2 and A_3 are constants which represent the fluorescence intensities of tRNA^{Leu}(Flu) at the posttranslocation State POST1, State POST2 and State POST3, respectively, relative to that at the pretranslocation state (including State H1, State H2 and State H3). Similarly, the change in FRET between S13(AttoQ) and tRNA^{Leu}(Flu) is calculated by

$$FRET_1(t) \propto 1 - P_1(t) - B_1\left[P_2(t) + P_3(t)\right] - B_2P_4(t) - B_3P_5(t) - B_4P_6(t), \tag{16}$$

where B_1, B_2, B_3 and B_4 are constants which represent FRETs at the state where the 30S head is rotated relative to the 30S body (including State H2 and State H3), at State POST1, at State POST2 and at State POST3, respectively, relative to that at the pre-translocation state where the 30S head is not rotated (State H1).

Based on the pathway of Fig. 1, the changes of tRNA^{Leu}(Flu) fluorescence and FRET between S13 and tRNA^{Leu}(Flu) for the case of two rounds of translocation can be resorted to Eqs. (9)–(13) supplemented by the following equations

$$\frac{dP_6(t)}{dt} = k_6P_5(t) - k_7P_6(t) - k_dP_6(t), \tag{17}$$

$$\frac{dP_7(t)}{dt} = k_7P_6(t) - k_8P_7(t) - k_dP_7(t), \tag{18}$$

with initial conditions (at $t = 0$) being as follows: $P_1(0) = 1$ and $P_i(0) = 0$ ($i = 2, \ldots, 7$). The change in the fluorescence of tRNA^{Leu}(Flu) is calculated by

$$Flu_2(t) \propto \left[P_1(t) + P_2(t) + P_3(t)\right] + A_1P_4(t) + A_2P_5(t) + A_3P_6(t) + A_4P_7(t), \tag{19}$$

where A_1, A_2 and A_3 have the same values as those defined in Eq. (15) and A_4 is a constant which represents the fluorescence intensity of tRNA^{Leu}(Flu) at State TC1 relative to that at the pre-translocation state (including State H1, State H2 and State H3). The change of FRET between S13 and tRNA^{Leu}(Flu) is calculated by

$$FRET_2(t) \propto 1 - P_1(t) - B_1\left[P_2(t) + P_3(t)\right] - B_2P_4(t) - B_3P_5(t) - B_4P_6(t) - B_5P_7(t), \tag{20}$$

where B_1, B_2, B_3 and B_4 have the same values as those defined in Eq. (16) and B_5 is a constant which represents FRET at State TC1 relative to that at the pretranslocation state where the 30S head is not rotated (State H1).

3.2. Equations for kinetics of –1 frameshifting with Model I

By comparing Fig. 2 with Fig. 1 it is seen that the pathway of –1 frameshifting for Model I is analogous to that for translation of –/– mRNA. Thus, we can use Eqs. (1)–(8) to study the change in FRET between L12 and EF-G for the translation of +/+ mRNA; use Eqs. (9)–(16) to study the changes of tRNA^{Leu}(Flu) fluorescence and FRET between S13 and tRNA^{Leu}(Flu) for the case of one round of translocation; and use Eqs. (9)–(13) and (17)–(20) to study the changes of tRNA^{Leu}(Flu) fluorescence and FRET between S13 and tRNA^{Leu}(Flu) for the case of two rounds of translocation. However, the incomplete translocation could induce the ribosomal complex to have different conformations in Fig. 2 from those in Fig. 1. Thus, the rate constants k_5, k_6, k_7 and k_8 for transitions in Fig. 2 could be significantly different from those in Fig. 1; the magnitudes A_1, A_2, A_3, A_4 and B_1, B_2, B_3, B_4, B_5 for states in Fig. 2 could also be different from those in Fig. 1; and the rate of tRNA^{Leu}(Flu) dissociation (k_d) from the posttranslocation state in Fig. 2 could also be significantly different from that in Fig. 1.

3.3. Equations for kinetics of –1 frameshifting with Model II

As the majority of the translating ribosomes frameshift (over 75%) [7], for approximation, only the frameshifting pathway is considered here. Based on our model (Figs. 3 and 4), for the case of one round of translocation the pathway of state transitions can be shown in Fig. 5. After EF-G.GDP release from the non-canonical rotated state (State FS1), in the absence of the ternary complexes EF-Tu.GTP.Phe-tRNA^{Phe} and EF-Tu.GTP.Val-tRNA^{Val}, EF-G.GTP binds to the ribosome (State FS1a). Then, GTP hydrolysis (State FS1b) induces the forward 30S head rotation (State FS1d) with a low probability of P_U, while the forward 30S head rotation does not occur (State FS1c) with a high probability of $1–P_U$. If no 30S head rotation occurs, after Pi and EF-G.GDP release, State FS1c returns to State FS1. If the 30S head rotation occurs, the resultant ribosomal unlocking (State FS6) facilitates the reverse intersubunit rotation, making the ribosomal complex change to the non-rotated State FS7, where the peptidyl-tRNA in the “canonical” P/P conformation induces the ribosome to be non-labile, accelerating EF-G.GDP release (State FS70).

Denoting by P_i ($i = 0, 1, \ldots, 13$) the probabilities of states of Fig. 5, based on the pathway shown in Fig. 5, the change in FRET between L12 and EF-G can be characterized by

$$F_{EF-G} \propto P_0 + P_6 + P_{13}, \tag{21}$$

where P_0, P_6 and P_{13} are calculated from the following equations

$$\frac{dP_0(t)}{dt} = -k_1P_0(t), \tag{22}$$

$$\frac{dP_1(t)}{dt} = k_1P_0(t) - k_2P_1(t), \tag{23}$$

$$\frac{dP_2(t)}{dt} = k_2P_1(t) - k_3P_2(t), \tag{24}$$

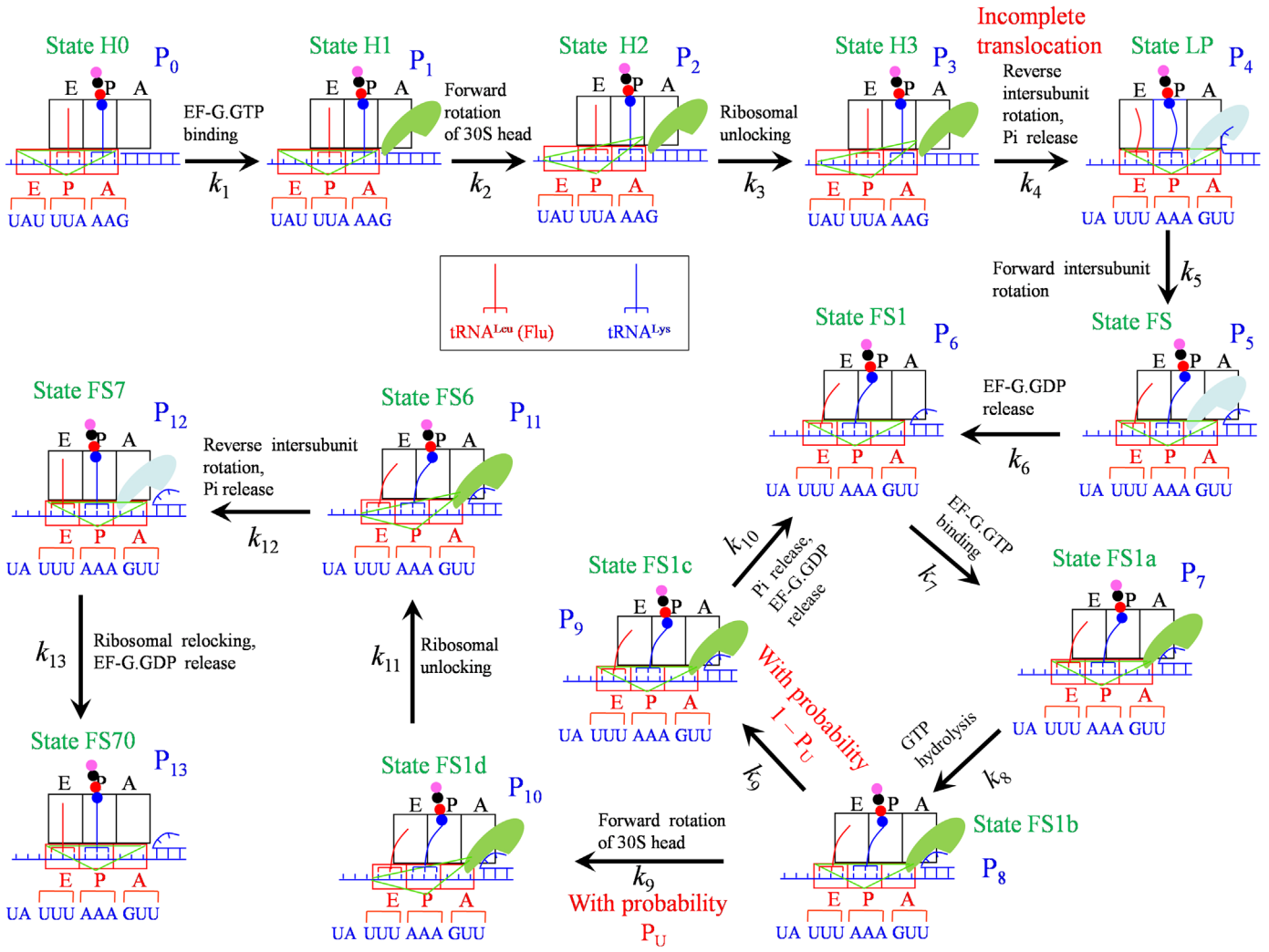

Fig. 5. Schematic representation of the –1 frameshifting pathway for the case of one round of translocation in Model II (see text for detailed description). Note that EF-G is in the elongated conformation.

$$\frac{dP_3(t)}{dt} = k_3P_2(t) - k_4P_3(t), \tag{25}$$

$$\frac{dP_4(t)}{dt} = k_4P_3(t) - k_5P_4(t), \tag{26}$$

$$\frac{dP_5(t)}{dt} = k_5P_4(t) - k_6P_5(t), \tag{27}$$

$$\frac{dP_6(t)}{dt} = k_6P_5(t) - k_7P_6(t) + k_{10}P_9(t), \tag{28}$$

$$\frac{dP_7(t)}{dt} = k_7P_6(t) - k_8P_7(t), \tag{29}$$

$$\frac{dP_8(t)}{dt} = k_8P_7(t) - k_9P_8(t), \tag{30}$$

$$\frac{dP_9(t)}{dt} = (1 - P_U)k_9P_8(t) - k_{10}P_9(t), \tag{31}$$

$$\frac{dP_{10}(t)}{dt} = P_Uk_9P_8(t) - k_{11}P_{10}(t), \tag{32}$$

$$\frac{dP_{11}(t)}{dt} = k_{11}P_{10}(t) - k_{12}P_{11}(t), \tag{33}$$

$$\frac{dP_{12}(t)}{dt} = k_{12}P_{11}(t) - k_{13}P_{12}(t), \tag{34}$$

$$\frac{dP_{13}(t)}{dt} = k_{13}P_{12}(t), \tag{35}$$

The initial conditions (at $t = 0$) for Eqs. (22)–(35) are imposed as follows, $P_0(0) = 1$ and $P_i(0) = 0$ ($i = 1, 2, \ldots, 13$).

Based on the pathway shown in Fig. 5, the changes of tRNA^{Leu}(Flu) fluorescence and FRET between S13 and tRNA^{Leu}(Flu) for the case of one round of translocation can be resorted to the following equations

$$\frac{dP_1(t)}{dt} = -k_2P_1(t), \tag{36}$$

$$\frac{dP_2(t)}{dt} = k_2P_1(t) - k_3P_2(t), \tag{37}$$

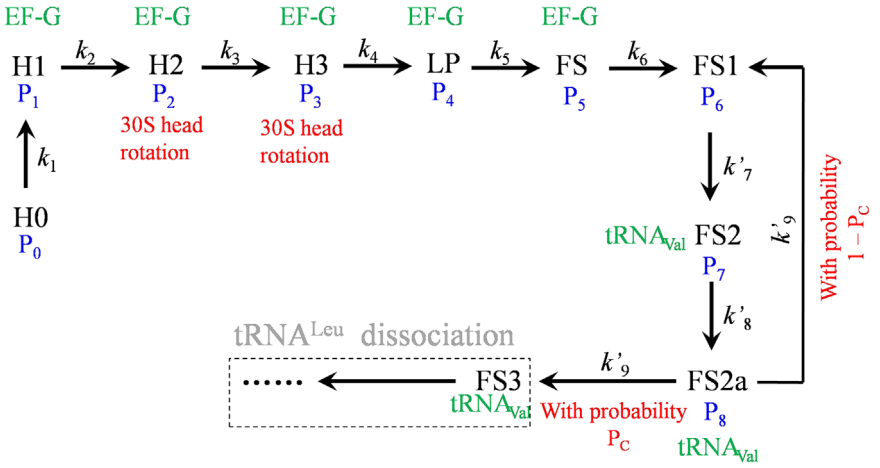

Fig. 6. Schematic representation of the –1 frameshifting pathway for the case of two rounds of translocation in Model II (see text for detailed description). Note that EF-G in State H1, State H2, State H3, State LP and State FS is in the elongated conformation.

$$\frac{dP_3(t)}{dt} = k_3P_2(t) - k_4P_3(t), \tag{38}$$

$$\frac{dP_4(t)}{dt} = k_4P_3(t) - k_5P_4(t) - k_{d1}P_4(t), \tag{39}$$

$$\frac{dP_5(t)}{dt} = k_5P_4(t) - k_6P_5(t) - k_{d1}P_5(t), \tag{40}$$

$$\frac{dP_6(t)}{dt} = k_6P_5(t) - k_7P_6(t) + k_{10}P_9(t) - k_{d1}P_6(t), \tag{41}$$

$$\frac{dP_7(t)}{dt} = k_7P_6(t) - k_8P_7(t) - k_{d1}P_7(t), \tag{42}$$

$$\frac{dP_8(t)}{dt} = k_8P_7(t) - k_9P_8(t) - k_{d1}P_8(t), \tag{43}$$

$$\frac{dP_9(t)}{dt} = (1 - P_U)k_9P_8(t) - k_{10}P_9(t) - k_{d1}P_9(t), \tag{44}$$

$$\frac{dP_{10}(t)}{dt} = P_Uk_9P_8(t) - k_{11}P_{10}(t) - k_{d2}P_{10}(t), \tag{45}$$

$$\frac{dP_{11}(t)}{dt} = k_{11}P_{10}(t) - k_{12}P_{11}(t) - k_{d2}P_{11}(t), \tag{46}$$

$$\frac{dP_{12}(t)}{dt} = k_{12}P_{11}(t) - k_{13}P_{12}(t) - k_{d3}P_{12}(t), \tag{47}$$

$$\frac{dP_{13}(t)}{dt} = k_{13}P_{12}(t) - k_{d3}P_{13}(t), \tag{48}$$

where k_{d1} is the rate of tRNA^{Leu}(Flu) dissociation after entering into the non-canonical states and before the forward rotation of the 30S head, k_{d2} is the rate of tRNA^{Leu}(Flu) dissociation with the forward rotation of the 30S head, and k_{d3} is the rate of tRNA^{Leu}(Flu) dissociation after the reverse intersubunit rotation (State FS7 and State FS70). Note that as State FS7 and State FS70 which result from the non-canonical rotated state in Fig. 5 could have different conformations from State POST1 and State POST2 which result from the canonical rotated state in Fig. 1, value of k_{d3} in Fig. 5 could be different from that of k_d in Fig. 1[6]. The change in the fluorescence of tRNA^{Leu}(Flu) is calculated by

$$Flu_1(t) \propto \sum_{i=1}^{3} P_i(t) + A_1P_4(t) + A_2\sum_{i=5}^{11} P_i(t) + A_3\left[P_{12}(t) + P_{13}(t)\right], \tag{49}$$

where A_1, A_2 and A_3 are constants which represent the fluorescence intensities of tRNA^{Leu}(Flu) at non-canonical non-rotated State LP, at non-canonical rotated states and at states after the reverse intersubunit rotation (including State FS7 and State FS70), respectively, relative to that at the pretranslocation state (including State H1, State H2 and State H3). Similarly, the changes in FRET between S13(AttoQ) and tRNA^{Leu}(Flu) is calculated by

$$FRET_1(t) \propto 1 - \left\{P_1(t) + B_1\left[P_2(t) + P_3(t)\right]\right\} - B_2P_4(t) - B_3\left\{\sum_{i=5}^{9} P_i(t) + B_1\left[P_{10}(t) + P_{11}(t)\right]\right\} - B_4\left[P_{12}(t) + P_{13}(t)\right], \tag{50}$$

where B_1, B_2, B_3 and B_4 are constants which represent FRETs at the state where the 30S head is rotated relative to the 30S body, at non-canonical non-rotated State LP, at non-canonical rotated states and at states after the reverse intersubunit rotation, respectively, relative to that at the pretranslocation state where the 30S head is not rotated (State H1).

Consider the case of two rounds of translocation. The single-molecule experimental data showed that the lifetime of EF-G bound to the non-canonical rotated states is much shorter than the lifetime of tRNA [4]. Thus, for approximation, we neglect the effect of EF-G.GTP binding to State FS1 in our studies of the changes of tRNA^{Leu}(Flu) fluorescence and FRET between S13 and tRNA^{Leu}(Flu). Then, from Figs. 3 and 4 the pathway for the case of two rounds of translocation is simplified to Fig. 6, where State FS2a represents the branching point from which the codon recognition occurs with a probability of P_C and the ternary complex is released with a probability of 1–P_C. Since after the codon recognition (State

[6] Note 6. This is consistent with the single-molecule experimental data of Chen et al. [4] showing that after the frameshifting the time of the elongation cycle is longer than that before the frameshifting. Moreover, in the several elongation cycles following the non-canonical state, the conformation of the ribosomal complex gradually returns to that of the canonical state.

FS3), tRNA^{Leu}(Flu) is considered to dissociate rapidly if it has not been dissociated yet due to the allosteric cooperation between the A and E sites [43–45], for simplicity, we do not need to consider the transitions after State FS3 in Fig. 6.

Based on Fig. 6, the changes of tRNA^{Leu}(Flu) fluorescence and FRET between S13 and tRNA^{Leu}(Flu) for the case of two rounds of translocation can be resorted to Eqs. (36) – (40) supplemented by the following equations

$$\frac{dP_6(t)}{dt} = k_6P_5(t) - k'_7P_6(t) + (1 - P_C)k'_9P_8(t) - k_{d1}P_6(t), \tag{51}$$

$$\frac{dP_7(t)}{dt} = k'_7P_6(t) - k'_8P_7(t) - k_{d1}P_7(t), \tag{52}$$

$$\frac{dP_8(t)}{dt} = k'_8P_7(t) - k'_9P_8(t) - k_{d1}P_8(t), \tag{53}$$

with initial conditions (at $t = 0$) being as follows: $P_1(0) = 1$ and $P_i(0) = 0$ ($i = 2, \ldots, 8$). The change in the fluorescence of tRNA^{Leu}(Flu) is calculated by

$$Flu_2(t) \propto \sum_{i=1}^{3} P_i(t) + A_1P_4(t) + A_2 \sum_{i=5}^{6} P_i(t) + A'_3[P_7(t) + P_8(t)], \tag{54}$$

where A_1 and A_2 have the same values as those defined in Eq. (49) and A'_3 is a constant which represents the fluorescence intensity of tRNA^{Leu}(Flu) after the binding of the ternary complex relative to that at the pretranslocation state (including State H1, State H2 and State H3). The change in FRET between S13 and tRNA^{Leu}(Flu) is calculated by

$$FRET_2(t) \propto 1 - \{P_1(t) + B_1[P_2(t) + P_3(t)]\} - B_2P_4(t) - B_3[P_5(t) + P_6(t)] - B'_4[P_7(t) + P_8(t)], \tag{55}$$

where B_1, B_2 and B_3 have the same values as those defined in Eq. (50) and B'_4 is a constant which represents FRET after the binding of the ternary complex relative to that at the pretranslocation state where the 30S head is not rotated (State H1). In this work, we use Runge-Kutta algorithm to numerically solve the differential equations.

4. Results

It is noted that in our models whether during translation of –/– mRNA (Fig. 1) or during translation of +/+ mRNA (Figs. 2 and 3) the rate constants of transitions from State H0 through State H3 have the same values. In addition, since in Model II (Fig. 3) the transition from State H3 to State POST1 or to State FC or to State LP is caused by the same reverse intersubunit rotation, the three transitions have the same rate constant, k_4. The values of these rate constants are chosen as follows. To be consistent with the experimental data of Caliskan et al. [7], we take EF-G.GTP-binding rate $k_1 = 5$ s^{-1} throughout our calculations. Based on the available biochemical data [20], the forward 30S head rotation is about 80 s^{-1}. Thus, we take $k_2 = 80$ s^{-1} throughout the calculations. From the available biochemical data [40], we take the ribosomal-unlocking rate $k_3 = 20$ s^{-1} in the calculations. As biochemical data showed that after the ribosomal unlocking the mRNA translocation or Pi release occurs rapidly [40], we take k_4 having a large value. For the calculation, we take $k_4 \geq 100$ s^{-1} (the variation of k_4 has nearly no effect on the results provided that k_4 has a large value).

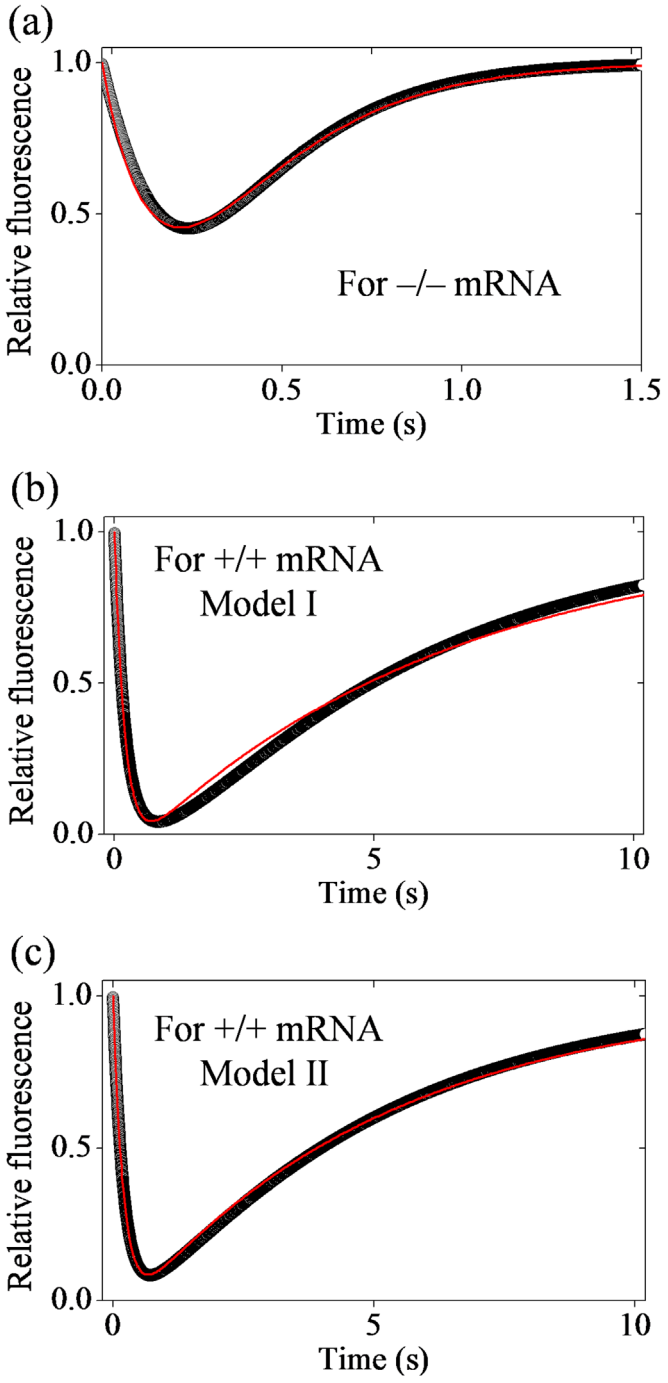

Fig. 7. Time courses of the change in FRET between L12 and EF-G, $F_{EF-G}(t)$. Symbols represent numerical results and red lines are fit by the two-exponential function, Eq. (56). (a) For –/– mRNA. $\lambda_1^{(G)} = 5$ s^{-1}, $\lambda_2^{(G)} = 4.2$ s^{-1} and $C = 8.5$. (b) For +/+ mRNA with Model I. $\lambda_1^{(G)} = 5$ s^{-1}, $\lambda_2^{(G)} = 0.164$ s^{-1} and $C = 1.11$. (c) For +/+ mRNA with Model II. $\lambda_1^{(G)} = 5$ s^{-1}, $\lambda_2^{(G)} = 0.2$ s^{-1} and $C = 1.09$.

4.1. Results for kinetics of translation of –/– mRNA

The choice of values of rate constants k_1, k_2, k_3 and k_4 has been discussed above. In the following we discuss the choice of other rate constants k_5, k_6, and k_d defined in Eqs. (2) – (14) and Fig. 1. The biochemical data showed that after the posttranslocation, the ribosome becomes non-labile with a rate of about 5 s^{-1}, which is followed by EF-G.GDP release, with a rate of about 20 s^{-1} [40]. Thus, we take $k_5 = 5$ s^{-1} and $k_6 = 20$ s^{-1}. The rate of tRNA^{Leu}(Flu) dissociation after the posttranslocation is taken to be $k_d = 3$ s^{-1},

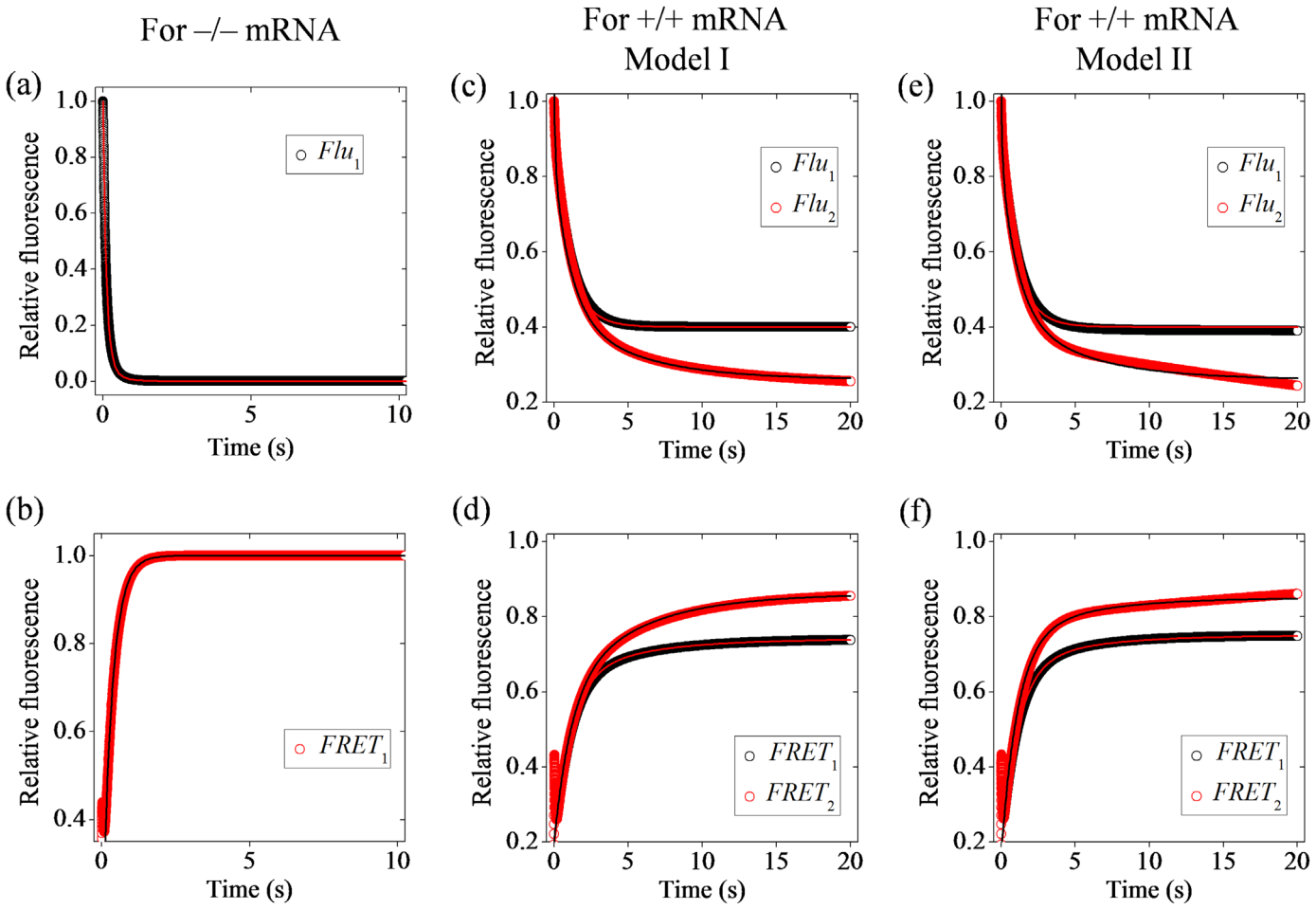

Fig. 8. Time courses of the changes in tRNA^{Leu}(Flu) fluorescence and FRET between S13(AttoQ) and tRNA^{Leu}(Flu). Symbols represent numerical results. $Flu_1(t)$ and $FRET_1(t)$ are the changes in tRNA^{Leu}(Flu) fluorescence and FRET between S13(AttoQ) and tRNA^{Leu}(Flu), respectively, for the case of one round of translocation, while $Flu_2(t)$ and $FRET_2(t)$ for the case of two rounds of translocation. (a, b) For –/– mRNA. The red line in (a) is fit by the two-exponential function, Eq. (57), with $\lambda_1 = 9\ s^{-1}$ and $\lambda_2 = 3\ s^{-1}$. The black line in (b) is fit by the two-exponential function, Eq. (58), with $\lambda_1 = 9\ s^{-1}$ and $\lambda_2 = 3\ s^{-1}$. (c, d) For +/+ mRNA with Model I. In (c) the red line is fit by the two-exponential function, Eq. (59), with $\lambda_1 = 11\ s^{-1}$, $\lambda_2 = 0.9\ s^{-1}$, $C_1 = 0.58$ and $C_2 = 0.4$, while the black line is fit by the three-exponential function, Eq. (61), with $\lambda_1 = 11\ s^{-1}$, $\lambda_2 = 0.9\ s^{-1}$, $\lambda_3 = 0.2\ s^{-1}$, $C'_1 = 0.76$ and $C'_2 = 0.26$. In (d) the red line is fit by the two-exponential function, Eq. (60), with $\lambda_2 = 0.9\ s^{-1}$, $\lambda_3 = 0.2\ s^{-1}$, $C_3 = 0.74$ and $C_4 = 0.56$, while the black line is fit by the two-exponential function, Eq. (62), with $\lambda_2 = 0.9\ s^{-1}$, $\lambda_3 = 0.2\ s^{-1}$, $C_3 = 0.86$ and $C_4 = 0.66$. (e, f) For +/+ mRNA with Model II. In (e) the red line is fit by the two-exponential function, Eq. (63), with $\lambda_1 = 11\ s^{-1}$, $\lambda_2 = 0.9\ s^{-1}$, $C_1 = 0.58$ and $C_2 = 0.4$, while the black line is fit by the three-exponential function, Eq. (65), with $\lambda_1 = 11\ s^{-1}$, $\lambda_2 = 0.9\ s^{-1}$, $\lambda_3 = 0.2\ s^{-1}$, $C'_1 = 0.76$ and $C'_2 = 0.26$. In (f) the red line is fit by the two-exponential function, Eq. (64), with $\lambda_2 = 0.9\ s^{-1}$, $\lambda_3 = 0.2\ s^{-1}$, $C_3 = 0.75$ and $C_4 = 0.58$, while the black line is fit by the two-exponential function, Eq. (66), with $\lambda_2 = 0.9\ s^{-1}$, $\lambda_3 = 0.2\ s^{-1}$, $C_3 = 0.85$ and $C_4 = 0.68$.

which is close to the value determined before by fitting to the single-molecule experimental data [47,48].

With Eqs. (1)–(8), we study the change in FRET between L12 and EF-G. The calculated results for the time course of the change in FRET, $F_{EF-G}(t)$, are shown in Fig. 7a. The theoretical data can be fit to the function

$$F_{EF-G}(t) = 1 - C\left[\exp\left(-\lambda_1^{(G)}t\right) - \exp\left(-\lambda_2^{(G)}t\right)\right], \tag{56}$$

where $\lambda_1^{(G)} = 5\ s^{-1}$, $\lambda_2^{(G)} = 4.2\ s^{-1}$ and C is a constant. These are consistent with the biochemical data (Fig. 2B in Caliskan et al. [7]).

With Eqs. (9)–(16), we study the changes in the fluorescence of tRNA^{Leu}(Flu) and FRET between S13(AttoQ) and tRNA^{Leu}(Flu) for the case of one round of translocation. The calculated results for the time courses of the change in tRNA^{Leu}(Flu) fluorescence, $Flu_1(t)$, and the change in FRET between S13(AttoQ) and tRNA^{Leu}(Flu), $FRET_1(t)$, are shown in Fig. 8a and b, respectively, where we take $A_1 = 0.45$, $A_2 = A_3 = 0.1$, $B_1 = 0.4$, and $B_2 = B_3 = B_4 = 0.8$. The calculated data of $Flu_1(t)$ versus t can be fit to the two-exponential function

$$Flu_1(t) = 0.89\exp(-\lambda_1 t) + 0.11\exp(-\lambda_2 t), \tag{57}$$

where $\lambda_1 = 9\ s^{-1}$ and $\lambda_2 = 3\ s^{-1}$. The results are in good agreement with the biochemical data (Fig. 4B and H in Caliskan et al. [7]). The calculated data of $FRET_1(t)$ versus t can be fit to the two-exponential function

$$FRET_1(t) = 1 - \left[0.1\exp(-\lambda_1 t) + 0.9\exp(-\lambda_2 t)\right], \tag{58}$$

where $\lambda_1 = 9\ s^{-1}$ and $\lambda_2 = 3\ s^{-1}$. The results are also in good agreement with the biochemical data (Fig. 4E and H in Caliskan et al. [7]).

4.2. Results for kinetics of –1 frameshifting with Model I

Values of rate constants k_1, k_2, k_3 and k_4 have been given above. Values of other rate constants k_5, k_6, k_7, k_8 and k_d defined in Eqs. (2)–(18) and Fig. 2 are adjusted to make the calculated data be consistent with the biochemical data [7], which are described as follows.

First, we use Eqs. (9)–(16) to study the changes in the fluorescence of tRNA^{Leu}(Flu), $Flu_1(t)$, and FRET between S13(AttoQ) and tRNA^{Leu}(Flu), $FRET_1(t)$, for the case of one round of translocation. We adjust the rate constant of the ribosome becoming non-labile

after posttranslocation to be $k_5 = 0.9\ s^{-1}$, the rate constant of EF-G. GDP release after the ribosome becoming non-labile to be $k_6 = 0.2\ s^{-1}$ and the rate constant of tRNA^{Leu}(Flu) dissociation after posttranslocation to be $k_d = 0$. The calculated results of $Flu_1(t)$ and $FRET_1(t)$ versus time t are shown in Fig. 8c and d, respectively, where we take $B_1 = 0.4$ that is the same as that taken in Fig. 8b, $A_1 = 0.9$, $A_2 = A_3 = 0.4$, $B_2 = 0.8$, $B_3 = 0.35$ and $B_4 = 0.26$. The calculated data of $Flu_1(t)$ versus t can be fit to the two-exponential function

$$Flu_1(t) = \left[0.22\exp(-\lambda_1 t) + 0.78\exp(-\lambda_2 t)\right]C_1 + C_2, \quad (59)$$

where $\lambda_1 = 11\ s^{-1}$, $\lambda_2 = 0.9\ s^{-1}$, and C_1 and C_2 are constants. The calculated data of $FRET_1(t)$ versus t can also be fit to the two-exponential function

$$FRET_1(t) = C_3 - C_4\left[0.8\exp(-\lambda_2 t) + 0.2\exp(-\lambda_3 t)\right], \quad (60)$$

where $\lambda_2 = 0.9\ s^{-1}$, $\lambda_3 = 0.2\ s^{-1}$, and C_3 and C_4 are constants. These results are in good agreement with the experimental data (Fig. 4C, F and I in Caliskan et al. [7]).

Then, we use Eqs. (9)–(13) and (17)–(20) to study the changes in tRNA^{Leu}(Flu) fluorescence, $Flu_2(t)$, and FRET between S13(AttoQ) and tRNA^{Leu}(Flu), $FRET_2(t)$, for the case of two rounds of translocation. Values of $k_5 = 0.9\ s^{-1}$, $k_6 = 0.2\ s^{-1}$ and $k_d = 0$ are the same as those for the case of one round of translocation. We take the binding rate of the ternary complex EF-Tu.GTP.Val-tRNA^{Val} to be $k_7 = 10\ s^{-1}$ (the variation of the value of k_7 has nearly no effect on the results provided that $k_7 \geq 10\ s^{-1}$). We adjust the rate constant of the codon recognition to be $k_8 = 0.005\ s^{-1}$. The calculated results of $Flu_2(t)$ and $FRET_2(t)$ versus time t are shown in Fig. 8c and d, respectively, where values of A_1, A_2, A_3, B_1, B_2, B_3 and B_4 are the same as those for the case of one round of translocation and in addition, we take $A_4 = 0.27$ and $B_5 = 0.15$. The calculated data of $Flu_2(t)$ versus t can be fit to the three-exponential function

$$Flu_2(t) = C'_1\left[0.25\exp(-\lambda_1 t) + 0.5\exp(-\lambda_2 t) + 0.25\exp(-\lambda_3 t)\right] + C'_2, \quad (61)$$

where $\lambda_1 = 11\ s^{-1}$, $\lambda_2 = 0.9\ s^{-1}$, $\lambda_3 = 0.2\ s^{-1}$, and C'_1 and C'_2 are constants. The calculated data of $FRET_2(t)$versus t can be fit to the two-exponential function

$$FRET_2(t) = C'_3 - C'_4\left[0.58\exp(-\lambda_2 t) + 0.42\exp(-\lambda_3 t)\right], \quad (62)$$

where $\lambda_2 = 0.9\ s^{-1}$, $\lambda_3 = 0.2\ s^{-1}$, and C'_3 and C'_4 are constants. These results are in agreement with the experimental data (Fig. 4C, F and I in Caliskan et al. [7]). Furthermore, from Fig. 8c and d we see that for the case of two rounds of translocation the tRNA^{Leu}(Flu) fluorescence has a further decrease and the FRET between S13(AttoQ) and tRNA^{Leu}(Flu) has a further increase compared to those for the case of one round of translocation, which are also in agreement with the biochemical data (Fig. 4C, F and I in Caliskan et al. [7]).

Third, we use Eqs. (1)–(8) to study the change in FRET between L12 and EF-G, which is characterized by $F_{EF-G}(t)$. With values of the rate constants as taken above, the calculated results of $F_{EF-G}(t)$ versus time t are shown in Fig. 7b, which can be approximately fit to the function described by Eq. (56), where $\lambda_1^{(G)} = 5\ s^{-1}$ and $\lambda_2^{(G)} = 0.164\ s^{-1}$. These are consistent with the biochemical data (Fig. 2C in Caliskan et al. [7]).

4.3. Results for kinetics of –1 frameshifting with Model II

First, we use Eqs. (36)–(50) to study the changes in the fluorescence of tRNA^{Leu}(Flu), $Flu_1(t)$, and FRET between S13(AttoQ) and tRNA^{Leu}(Flu), $FRET_1(t)$, for the case of one round of translocation. Values of rate constants k_1, k_2, k_3 and k_4 have been given above, while values of other rate constants k_i ($i = 5, 6, \ldots, 13$), k_{d1}, k_{d2} and k_{d3} defined in Eqs. (36)–(48) and Fig. 5 are chosen as follows. We take $k_5 = 0.9\ s^{-1}$, which is consistent with the smFRET data on the EF-G-facilitating forward ribosomal rotation [24,49]. The EF-G.GTP binding rate $k_7 = k_1 = 5\ s^{-1}$ for the concentration of EF-G.GTP used in the experiments of Caliskan et al. [7]. From the available biochemical data, we have GTP-hydrolysis rate $k_8 = 250\ s^{-1}$ [40], 30S-head-rotation rate $k_9 = k_2 = 80\ s^{-1}$ [20], ribosome-becoming-non-labile rate $k_{11} = k_3 = 20\ s^{-1}$ [40], reverse-intersubunit-rotation rate $k_{12} = k_4 \geq 100\ s^{-1}$ after the ribosomal unlocking [40], and rate of ribosome becoming non-labile and then EF-G.GDP release, $k_{13} = 4\ s^{-1}$ (with a rate of $5\ s^{-1}$ for ribosome becoming non-labile followed by release of EF-G.GDP of a rate of $20\ s^{-1}$) in the canonical posttranslocation state [40]. To be consistent with the single-molecule data showing that the lifetime of EF-G bound to the non-canonical long-paused state is about 0.9 s [4], we take $k_{10} = k_6 = 1.4\ s^{-1}$ in the calculation (this value of rate constant of EF-G.GDP release from the non-canonical long-paused state, together with the above values of k_8 and k_9, give the mean lifetime of EF-G bound to the non-canonical state to be close to 0.9 s). To be consistent with the single-molecule data with the number of EF-G.GTP bindings to the long-paused rotated state being about 5 [4], we take the probability $P_u = 0.2$. In addition, we adjust $k_{d1} = k_{d2} = k_{d3} = 0$. The calculated results of $Flu_1(t)$ and $FRET_1(t)$ versus time t are shown in Fig. 8e and f, respectively, where we take $A_1 = 0.9$, $A_2 = A_3 = 0.4$, $B_1 = 0.4$ that is the same as that taken in Fig. 8b, $B_2 = 0.8$, $B_3 = 0.32$ and $B_4 = 0.25$. The calculated data of $Flu_1(t)$ versus t can be fit to the two-exponential function,.

$$Flu_1(t) = \left[0.22\exp(-\lambda_1 t) + 0.78\exp(-\lambda_2 t)\right]C_1 + C_2, \quad (63)$$

where $\lambda_1 = 11\ s^{-1}$, $\lambda_2 = 0.9\ s^{-1}$, and C_1 and C_2 are constants. The calculated data of $FRET_1(t)$ versus t can also be fit to the two-exponential function

$$FRET_1(t) = C_3 - C_4\left[0.85\exp(-\lambda_2 t) + 0.15\exp(-\lambda_3 t)\right], \quad (64)$$

where $\lambda_2 = 0.9\ s^{-1}$, $\lambda_3 = 0.2\ s^{-1}$, and C_3 and C_4 are constants. These results are in good agreement with the biochemical data (Fig. 4C, F and I in Caliskan et al. [7]).

Then, we use Eqs. (36)–(40) and Eqs. (51)–(55) to study the changes in fluorescence of tRNA^{Leu}(Flu), $Flu_2(t)$, and FRET between S13(AttoQ) and tRNA^{Leu}(Flu), $FRET_2(t)$, for the case of two rounds of translocation (Fig. 6). As mentioned above, we take $k_5 = 0.9\ s^{-1}$, $k_6 = 1.4\ s^{-1}$ and $k_{d1} = 0$, which are the same as those for the case of one round of translocation. In addition, we take the binding rate of the ternary complex EF-Tu.GTP.Val-tRNA^{Val} to be $k'_7 = 10\ s^{-1}$ (the variation of the value of k'_7 has nearly no effect on the results provided that $k'_7 \geq 10\ s^{-1}$). To be consistent with the single-molecule data showing that the sampling number of the aminoacyl-tRNA to the non-canonical rotated state is about 2 and the sampling time is about 30 s [4], we take $P_C = 0.5$ and $k'_8 = 0.04\ s^{-1}$. For the calculation, we take k'_9 (corresponding to the rate constant of deacylated-tRNA dissociation from the E site after the codon recognition in the A-site) having a large value, e.g., $k'_9 \geq 100\ s^{-1}$. The calculated results of $Flu_2(t)$ and $FRET_2(t)$ versus time t are shown in Fig. 8e and f, respectively, where values of A_1, A_2, B_1, B_2 and B_3 are the same as those for the case of one round of translocation and in addition, we take $A'_3 = 0.35$ and $B'_4 = 0.2$. The theoretical data of $Flu_2(t)$ versus t can be fit to the three-exponential function

$$Flu_2(t) = C'_1\left[0.25\exp(-\lambda_1 t) + 0.5\exp(-\lambda_2 t) + 0.25\exp(-\lambda_3 t)\right] + C'_2, \quad (65)$$

where $\lambda_1 = 11\ s^{-1}$, $\lambda_2 = 0.9\ s^{-1}$, $\lambda_3 = 0.2\ s^{-1}$, and C'_1 and C'_2 are constants. The theoretical data of $FRET_2(t)$ versus t can be fit to the two-exponential function

$$FRET_2(t) = C'_3 - C'_4\left[0.83\exp(-\lambda_2 t) + 0.17\exp(-\lambda_3 t)\right], \quad (66)$$

where $\lambda_2 = 0.9\ s^{-1}$, $\lambda_3 = 0.2\ s^{-1}$, and C'_3 and C'_4 are constants. These are in agreement with the experimental data (Fig. 4C, F and I in Caliskan et al. [7]). Furthermore, it is seen that for the case of two rounds of translocation the tRNA^{Leu}(Flu) fluorescence has a further decrease and the FRET between S13(AttoQ) and tRNA^{Leu}(Flu) has a further increase compared to those for the case of one round of translocation, which are also in agreement with the biochemical data (Fig. 4C, F and I in Caliskan et al. [7]).

In addition, by comparing Fig. 8a with Fig. 8e it is seen that the relative magnitude of $Flu_1(t)$ with −/− mRNA to those of $Flu_1(t)$ and $Flu_2(t)$ with +/+ mRNA is also in good agreement with the biochemical data (Fig. 4 in Caliskan et al. [7]). Similarly, by comparing Fig. 8b with 8f we see that the relative magnitude of $FRET_1(t)$ with −/− mRNA to those of $FRET_1(t)$ and $FRET_2(t)$ with +/+ mRNA is also in good agreement with the biochemical data (Fig. 4 in Caliskan et al. [7]).

Finally, with Eqs. (21)–(35) and values of parameters given above, we calculate $F_{EF-G}(t)$, with the results shown in Fig. 7c. The calculated data can be fit to the function described by Eq. (56) where $\lambda_1^{(G)} = 5\ s^{-1}$ and $\lambda_2^{(G)} = 0.2\ s^{-1}$. These results are also in good agreement with the experimental data (Fig. 2C in Caliskan et al. [7]).

4.4. Model II is more reasonable than Model I

From Fig. 8c, d, e and f we note that both Model I and Model II can give quantitative explanations of the biochemical data of Caliskan et al. [7]. However, it is noted that in order to make the theoretical data be consistent with the biochemical data, in Model I it is required that the mean lifetime of an EF-G molecule bound to the ribosome is $T_{EF-G} = 1/k_2 + 1/k_3 + 1/k_4 + 1/k_5 + 1/k_6 \approx 6.2$ s and the mean lifetime of one tRNA^{Val} sampling event is $T_{tRNA} > 1/k_8 = 200$ s (see Fig. 2). By comparison, the single-molecule experimental data showed that the mean lifetime of an EF-G molecule bound to the non-canonical state is about 0.9 s and the mean lifetime of one tRNA sampling event to the non-canonical state is about 30 s [4]. The theoretical data of T_{EF-G} and T_{tRNA} are about 7-fold larger than the corresponding experimental data. Moreover, the very small rate constant of codon recognition, $k_8 = 0.005\ s^{-1}$, in Fig. 2 implies that the rate of Val incorporation is about $0.005\ s^{-1}$, which is much smaller than the biochemical data of about 0.06–0.3 s^{-1} [7].

By contrast, in Model II values of all rate constants k_i ($i = 1, \ldots, 13$), k'_7, k'_8 and k'_9, probability P_u and probability P_C defined in Figs. 5 and 6 are consistent with the available biochemical and single-molecule data [4,20,24,40]. These give the mean lifetime of an EF-G molecule bound to the non-canonical long paused state (about 0.9 s) and the mean lifetime of one tRNA^{Val} sampling event to the non-canonical long paused state ($T_{tRNA} \approx 1/k'_8 = 25$ s) to be consistent with the single-molecule data of about 0.9 s and 30 s, respectively [4]. The observed long lifetime of EF-G bound to the ribosome by Caliskan et al. [7] results from multiple EF-G cycles in Model II (Fig. 5). In addition, the rate constant of codon recognition in the long-paused rotated state, $k'_8 = 0.04\ s^{-1}$, and probability $P_C = 0.5$ (see Fig. 6) give the rate of Val incorporation to be about $0.02\ s^{-1}$, which is also close to the experimental data of about 0.06–0.3 s^{-1} [7]. Thus, we think that Model II is more reasonable than Model I to describe the pathway of the −1 frameshifting in the classic systems studied in Caliskan et al. [7].

5. Discussion

It is noted that for both Model I and Model II, in order to make the theoretical data be consistent with the experimental data, it is required that for the +/+ mRNA the rate of tRNA^{Leu}(Flu) dissociation from the non-canonical state in one round of translocation is equal or nearly equal to zero. Thus, the change in tRNA^{Leu}(Flu) fluorescence in one round of translocation does not result from the dissociation of tRNA^{Leu}(Flu), rather it results from the conformational change of the ribosomal complex. To see if the dissociation of tRNA^{Leu}(Flu) can occur in one round of translocation, it is interesting to study the effect of tRNA^{Leu}(Flu) dissociation on the changes in tRNA^{Leu}(Flu) fluorescence and in FRET between S13(AttoQ) and tRNA^{Leu}(Flu) and compare with the biochemical data.

5.1. The argument that the observed decrease of tRNA^{Leu}(Flu) fluorescence during the translation of +/+ mRNA results from the dissociation of tRNA^{Leu}(Flu) is unreasonable

Consider that the decrease of tRNA^{Leu}(Flu) fluorescence during the translation of +/+ mRNA observed in the experiments [7] results from the dissociation of tRNA^{Leu}(Flu) and the conformational change of the ribosomal complex has no effect on tRNA^{Leu}(Flu) fluorescence. To calculate the fluorescence change, we consider the pathway shown in Fig. 2, where tRNA^{Leu}(Flu) can be dissociated from the ribosome after transition to State POST1. The dissociation rates from State POST1, State POST2 and State POST3 are denoted by k_{d1}, k_{d2} and k_{d3}, respectively. After the binding of EF-Tu.GTP.Val-tRNA^{Val} and before the codon recognition, the dissociation rate is still represented by k_{d3}. Then, based on the pathway (Fig. 2), for the case of one round of translocation the temporal evolution of the state probabilities P_1, P_2, P_3, P_4, P_5 and P_6 can be described by Eqs. (S5)–(S10) (see Section S2) and the change in the tRNA^{Leu}(Flu) fluorescence can be calculated by $Flu_1 \propto \sum_{i=1}^{6} P_i$. For the case of two rounds of translocation, since after the codon recognition (State TC2) tRNA^{Leu}(Flu) is considered to dissociate rapidly due to the allosteric cooperation between the A and E sites [43–45], for simplicity, we do not consider the transitions after State TC2 in Fig. 2. Thus, for the case of two rounds of translocation the temporal evolution of the state probabilities P_1, P_2, P_3, P_4, P_5, P_6 and P_7 can be described by Eqs. (S5)–(S9), (S12) and (S13) (see Section S2) and the change in the tRNA^{Leu}(Flu) fluorescence can be calculated by $Flu_2 \propto \sum_{i=1}^{7} P_i$.

In order to make the calculated results be consistent with the experimental data (Fig. S3a), we adjust the rate constant of tRNA^{Leu}(Flu) dissociation from State POST1 to be $k_{d1} = 1\ s^{-1}$, from State POST2 to be $k_{d2} = 0.065\ s^{-1}$ and from State POST3 or State TC1 to be $k_{d3} = 0$, and the rate constant of the codon recognition, $k_8 = 0.05\ s^{-1}$, while the rate constants k_i ($i = 2, \ldots, 7$) are the same as those used to obtain the results shown in Fig. 8c and d. It is puzzling that while in State POST1 the dissociation rate k_{d1} is $1\ s^{-1}$, after the ribosome becoming non-labile the dissociation rate k_{d2} is reduced to $0.065\ s^{-1}$ and moreover, after the EF-G.GDP release the dissociation rate k_{d3} becomes zero. By contrast, it is more reasonable that the three dissociation rates should have the relation, $k_{d1} \le k_{d2} \le k_{d3}$, and thus, if $k_{d3} = 0$, k_{d1} and k_{d2} should also be zero. In fact, even for a small value of $k_{d1} = k_{d2} = k_{d3} = 0.2\ s^{-1}$, the tRNA^{Leu}(Flu) fluorescence for one round of translocation becomes nearly zero in 20 s (Fig. S3b), and thus, the further decreases in the tRNA^{Leu}(Flu) fluorescence would not be observed for two rounds of translocation, which is inconsistent with the experimental data [7]. Thus, the argument that the observed decrease of tRNA^{Leu}(Flu) fluorescence during the translation of +/+ mRNA results from the dissociation of tRNA^{Leu}(Flu) is unreasonable.

5.2. Concluding remarks

In summary, we present two models (Model I and Model II) to quantitatively explain the biochemical data of Caliskan et al. [7] on

the change in FRET between L12 and EF-G, the change in $tRNA^{Leu}$(Flu) fluorescence and the change in FRET between S13 (AttoQ) and $tRNA^{Leu}$(Flu) during translation of the +/+ mRNA. The further analysis showed that Model II is more reasonable than Model I to describe the pathway of the −1 translational frameshifting. In addition, it should be mentioned that Model II is much similar to that proposed in the previous work [14] except that the intrasubunit 30S head rotations are not included in Ref. [14]. In the previous works [14,15], the single-molecule experimental data of Chen et al. [4] on the dynamics of long pausing associated with the −1 frameshifting, the experimental data of Yan et al. [47] on multiple translocation excursions and broad branching of frameshifting pathways, and the single-molecule FRET data of Kim et al. [6] on multiple fluctuations between the non-rotated and rotated states of the ribosomal complex before undergoing mRNA translocation were explained quantitatively. Thus, we note that the diverse experimental data of Caliskan et al. [7], Chen et al. [4], Yan et al. [6] and Kim et al. [5] can be explained consistently by the very similar pathway and mechanism, as described by Model II.

Acknowledgments

This work was supported by the National Natural Science Foundation of China (Grant no. 11374352).

Appendix A. Transparency document

Transparency document associated with this article can be found in the online version at http://dx.doi.org/10.1016/j.bbrep.2016.02.008.

References

[1] P.J. Farabaugh, Programmed translational frameshifting, Microbiol. Rev. 60 (1996) 103–134.
[2] J.D. Dinman, Mechanisms and implications of programmed translational frameshifting, Wiley Interdiscip. Rev. RNA 3 (2012) 661–673.
[3] J.A. Dunkle, C.M. Dunham, Mechanisms of mRNA frame maintenance and its subversion during translation of the genetic code, Biochimie 114 (2015) 90–96.
[4] J. Chen, A. Petrov, M. Johansson, A. Tsai, S.E. O'Leary, J.D. Puglisi, Dynamic pathways of −1 translational frameshifting, Nature 512 (2014) 328–332.
[5] H.-K. Kim, F. Liu, J. Fei, C. Bustamante, R.L. Gonzalez Jr, I. Tinoco Jr, A frameshifting stimulatory stem loop destabilizes the hybrid state and impedes ribosomal translocation, Proc. Natl. Acad. Sci. USA 111 (2014) 5538–5543.
[6] S. Yan, J.-D. Wen, C. Bustamante, I. Tinoco, Ribosome excursions during mRNA translocation mediate broad branching of frameshift pathways, Cell 160 (2015) 870–881.
[7] N. Caliskan, V.I. Katunin, R. Belardinelli, F. Peske, M.V. Rodnina, Programmed −1 frameshifting by kinetic partitioning during impeded translocation, Cell 157 (2014) 1619–1631.
[8] E.P. Plant, K.L.M. Jacobs, J.W. Harger, A. Meskauskas, J.L. Jacobs, J.L. Baxter, A. N. Petrov, J.D. Dinman, The 9-Å solution: how mRNA pseudoknots promote efficient programmed −1 ribosomal frameshifting, RNA 9 (2003) 168–174.
[9] B.L. Bailey, K. Visscher, J. Watkins, A stochastic model of translation with −1 programmed ribosomal frameshifting, Phys. Biol. 11 (2014) (2014) 016009.
[10] M. Leger, D. Dulude, S.V. Steinberg, L. Brakier-Gingras, The three transfer RNAs occupying the A, P and E sites on the ribosome are involved in viral programmed −1 ribosomal frameshift, Nucleic Acids Res. 35 (2007) 5581–5592.
[11] O. Namy, S.J. Moran, D.I. Stuart, R.J. Gilbert, I. Brierley, A mechanical explanation of RNA pseudoknot function in programmed ribosomal frameshifting, Nature 441 (2006) 244–247.
[12] P.-Y. Liao, Y.S. Choi, J.D. Dinman, K.L. Lee, The many paths to frameshifting: kinetic modeling and analysis of the effects of different elongation steps on programmed −1 ribosomal frameshifting, Nucleic Acids Res. 39 (2011) 300–312.
[13] P. Xie, A dynamical model of programmed −1 ribosomal frameshifting, J. Theor. Biol. 336 (2013) 119–131.
[14] P. Xie, Model of the pathway of −1 frameshifting: long pausing, Biochem. Biophys. Rep. 5 (2016) 408–424.
[15] P. Xie, Origin of multiple intersubunit rotations before EF-G-catalyzed ribosomal translocation through the mRNA with a downstream secondary structure, BMC Biophys. 7 (2014) 12.
[16] D.J. Taylor, J. Nilsson, A.D. Merrill, G.R. Andersen, P. Nissen, J. Frank, Structures of modified eEF2.80S ribosome complexes reveal the role of GTP hydrolysis in translocation, EMBO J. 26 (2007) 2421–2431.
[17] A.H. Ratje, J. Loerke, A. Mikolajka, et al., Head swivel on the ribosome facilitates translocation by means of intra-subunit tRNA hybrid sites, Nature 468 (2010) 713–716.
[18] D.J. Ramrath, L. Lancaster, T. Sprink, T. Mielke, J. Loerke, H.F. Noller, C.M. T. Spahn, Proc. Natl. Acad. Sci. U. S. A. 110 (2013) 20964–20969.
[19] J. Zhou, L. Lancaster, J.P. Donohue, H.F. Noller, Crystal structures of EF-G-ribosome complexes trapped in intermediate states of translocation, Science 340 (2013) 1236086.
[20] Z. Guo, H.F. Noller, Rotation of the head of the 30S ribosomal subunit during mRNA translocation, Proc. Natl. Acad. Sci. USA 109 (2012) 20391–20394.
[21] P. Xie, Model of ribosomal translocation coupled with intra- and inter-subunit rotations, Biochem. Biophys. Rep. 2 (2015) 87–93.
[22] S.C. Blanchard, H.D. Kim, R.L. Gonzalez Jr., J.D. Puglisi, S. Chu., tRNA dynamics on the ribosome during translation, Proc. Natl. Acad. Sci. USA 101 (2004) 12893–12898.
[23] J. Fei, P. Kosuri, D.D. MacDougall, R.L. Gonzalez Jr., Coupling of ribosomal L1 stalk and tRNA dynamics during translation elongation, Mol. Cell 30 (2008) 348–359.
[24] P.V. Cornish, D.N. Ermolenko, H.F. Noller, T. Ha, Spontaneous intersubunit rotation in single ribosomes, Mol. Cell 30 (2008) 578–588.
[25] C. Chen, B. Stevens, J. Kaur, D. Cabral, H. Liu, Y. Wang, H. Zhang, G. Rosenblum, Z. Smilansky, Y.E. Goldman, B. Cooperman, Single-molecule fluorescence measurements of ribosomal translocation dynamics, Mol. Cell 42 (2011) 367–377.
[26] J. Chen, A. Petrov, A. Tsai, S.E. O'Leary, J.D. Puglisi, Coordinated conformational and compositional dynamics drive ribosome translocation, Nat. Struct. Mol. Biol. 20 (2013) 718–727.
[27] P. Xie, Translocation dynamics of tRNA-mRNA in the ribosome, Biophys. Chem. 180-181 (2013) 22–28.
[28] J. Lin, M.G. Gagnon, D. Bulkley, T.A. Steitz, Conformational changes of elongation factor G on the ribosome during tRNA translocation, Cell 160 (2015) 219–227.
[29] M. Selmer, C.M. Dunham, F.V. Murphy, A. Weixlbaumer, S. Petry, A.C. Kelley, J. R. Weir, V. Ramakrishnan, Structure of the 70S ribosome complexed with mRNA and tRNA, Science 313 (2006) 1935–1942.
[30] J.A. Dunkle, L. Wang, M.B. Feldman, et al., Structures of the bacterial ribosome in classical and hybrid states of tRNA binding, Science 332 (2011) 981–984.
[31] L.B. Jenner, N. Demeshkina, G. Yusupova, M. Yusupov, Structural aspects of messenger RNA reading frame maintenance by the ribosome, Nat. Struct. Mol. Biol. 17 (2010) 555–560.
[32] R.E. Stanley, G. Blaha, R.L. Grodzicki, M.D. Strickler, T.A. Steitz, The structures of the anti-tuberculosis antibiotics viomycin and capreomycin bound to the 70S ribosome, Nat. Struct. Mol. Biol. 17 (2010) 289–293.
[33] S. Feng, Y. Chen, Y.-G. Gao, Crystal structure of 70S ribosome with both cognate tRNAs in the E and P sites representing an authentic elongation complex, PLoS One 8 (2013) e58829.
[34] Y.-G. Gao, M. Selmer, C.M. Dunham, A. Weixlbaumer, A.C. Kelley, V. Ramakrishnan, The structure of the ribosome with elongation factor G trapped in the posttranslocational state, Science 326 (2009) 694–699.
[35] M.M. Yusupov, G.Z. Yusupova, A. Baucom, K. Lieberman, T.N. Earnest, J.H. D. Cate, H.F. Noller, Crystal structure of the ribosome at 5.5 A resolution, Science 292 (2001) 883–896.
[36] M. Laurberg, H. Asahara, A. Korostelev, J.Y. Zhu, S. Trakhavov, H.F. Noller, Structural basis for translation termination on the 70S ribosome, Nature 454 (2008) 852–857.
[37] A. Korostelev, H. Asahara, L. Lancaster, et al., Crystal structure of a translation termination complex formed with release factor RF2, Proc. Natl. Acad. Sci. USA 105 (2008) 19684–19689.
[38] R. Lill, J.M. Robertson, W. Wintermeyer, Binding of the 30-terminus of tRNA to 23S rRNA in the ribosomal exit site actively promotes translocation, EMBO J. 8 (1989) 3933–3938.
[39] J.S. Feinberg, S. Joseph, Identification of molecular interactions between P-site tRNA and the ribosome essential for translocation, Proc. Natl. Acad. Sci. USA 98 (2001) 11120–11125.
[40] A. Savelsbergh, V.I. Katunin, D. Mohr, F. Peske, M.V. Rodnina, W. Wintermeyer, An elongation factor G-induced ribosome rearrangement precedes tRNA-mRNA translocation, Mol. Cell 11 (2003) 1517–1523.
[41] P. Xie, A unified model of nucleic acid unwinding by the ribosome and the hexameric and monomeric DNA helicases, J. Theor. Biol. 380 (2015) 359–366.
[42] P. Xie, Dwell-time distribution, long pausing and arrest of single-ribosome translation through the mRNA duplex, Int. J. Mol. Sci. 16 (2015) 23723–23744.
[43] F. Robert, L. Brakier-Gingras, A functional interaction between ribosomal proteins S7 and S11 within the bacterial ribosome, J. Biol. Chem. 278 (2003) 44913–44920.
[44] G. Dinos, D.N. Wilson, Y. Teraoka, W. Szaflarski, P. Fucini, D. Kalpaxis, K. H. Nierhaus, Dissecting the ribosomal inhibition mechanisms of edeine and pactamycin: the universally conserved residues G693 and C795 regulate P-site

tRNA binding, Mol. Cell 13 (2004) 113–124.
[45] G. Dinos, D.L. Kalpaxis, D.N. Wilson, K.H. Nierhaus, Deacylated tRNA is released from the E site upon A site occupation but before GTP is hydrolyzed by EF-Tu, Nucleic Acids Res. 33 (2005) 5291–5296.
[46] P. Xie, Model of EF4-induced ribosomal state transitions and mRNA translocation, Phys. Biol. 11 (2014) 046007.
[47] P. Xie, Dynamics of tRNA occupancy and dissociation during translation by the ribosome, J. Theor. Biol. 316 (2013) 49–60.
[48] S. Uemura, C.E. Aitken, J. Korlach, B.A. Flusberg, S.W. Turner, J.D. Puglisi, Real-time tRNA transit on single translating ribosomes at codon resolution, Nature 464 (2010) 1012–1017.
[49] P. Xie, An explanation of biphasic characters of mRNA translocation in the ribosome, BioSystems 118 (2014) 1–7.